CO4-1

Radiation Effects on the Piezoelectric Response of PZT under 30 MeV Electron Irradiation

S. Takechi[1], S. Katayama[1], K. Nagasawa[1], S. Yamauchi[1], H. Horiuchi[2], Y. Horigami[2], M. Kobayashi[3], and T. Miyachi[3]

[1]*Graduate School of Engineering, Osaka Metropolitan University*
[2]*Faculty of Engineering, Osaka Metropolitan University*
[3]*Planetary Exploration Research Center, Chiba Institute of Technology*

INTRODUCTION: In this study, we investigate the potential application of piezoelectric elements for radiation measurement. The electromechanical coupling coefficient k — calculated from the resonant and antiresonant frequencies — is used as a key performance metric for these elements. Previous work reported changes in k when PZT elements were directly irradiated with high-energy Xe ion beams [1–3]. To clarify how k in PZT depends on radiation type, we are conducting irradiation experiments with a high-energy electron beam at KURNS-LINAC [4]. Because the k value of PZT tends to decrease above a certain temperature, continuous measurements under 20 MeV electron irradiation were performed on a single PZT element while minimizing thermal effects in fiscal years 2023–2024. Those results showed a monotonic decrease in k proportional to cumulative electron dose, with the reduced k persisting after irradiation ceased [5].

EXPERIMENTS: In the 2025 experiments, the electron energy was increased from 20 MeV to 30 MeV to investigate the effect of energy variation on the k value of PZT elements. Two campaigns were carried out (July and December 2025), each lasting three days, during which a 30 MeV electron beam irradiated PZT piezoelectric elements. Beam current was adjusted to keep the element surface temperature within a range where thermal effects could be neglected. The PZT elements were disk-shaped (radius 9 mm, thickness 1 mm), identical in specification to those used previously. Surface temperature was monitored continuously with thermocouples during irradiation. Each irradiation lasted approximately 15 minutes; frequency–impedance measurements were performed only after the element surface temperature had returned close to room temperature. Measurements were taken six times per day to obtain sufficient data points.

RESULTS: Irradiation of a single PZT element with a 30 MeV electron beam over several days produced a monotonic decrease in k with cumulative dose. The reduced k persisted during irradiation interruptions. Comparison with the 20 MeV data indicates a different rate of k decrease for the same cumulative dose. Future work will include additional experiments varying electron energy to examine these differences in detail.

REFERENCES:

[1] M. Kobayashi *et al*., Japanese Journal of Applied Physics, *52* (2013) 126604/1-5.
[2] M. Kobayashi *et al.*, Japanese Journal of Applied Physics, *53* (2014) 066602/1-6.
[3] S. Takechi *et al.*, Japanese Journal of Applied Physics, *60* (2021) 038003/1-3.
[4] S. Takechi *et al*., Japanese Journal of Applied Physics, *61* (2022) 128001/1-3.
[5] S. Takechi *et al*., Japanese Journal of Applied Physics, *63* (2024) 078002/1-4.

CO4-2

Characterization of Ni-Si nanoparticles precipitated in Cu-Ni-Si alloy using Small-Angle X-ray Scattering

Y. Oba[1], H. Sasaki [2]

[1] *Department of Mechanical Engineering, Toyohashi University of Technology*
[2] *Furukawa Electric Co., Ltd.*

INTRODUCTION: Cu-Ni-Si alloy is renowned precipitation-strengthened Cu alloys and is widely used as electrodes in electronic devices. Recent progress of miniaturization in the electronic devices requires further strengthening and higher conductivity for the Cu-Ni-Si alloy. In this alloy, Ni-Si nanoparticles are precipitated in Cu matrix and improve the mechanical strength. In contrast, solute Ni and Si reduce the electric conductivity. Therefore, the precise control of precipitation by aging heat treatment is an important issue. Small-angle X-ray scattering (SAXS) can quantitatively characterize the shape and amount of such nanoscale precipitates in alloys and provide useful knowledge for precipitation mechanism [1,2]. Therefore, the SAXS measurements of the Ni-Si precipitates in Cu-Ni-Si alloy was conducted in this study.

EXPERIMENTS: The Cu-Ni-Si alloy was first solution-treated and then aged at the temperature between 623 and 773 K. The SAXS measurements were performed using the SAXS instrument (NANO-Viewer, Rigaku) with Mo Kα radiation. Scattering patterns were measured using a photon-counting-type two-dimensional detector (PILATUS 100k, Dectris) using a Si converter with the thickness of 1000 μm. The X-ray path from the X-ray entrance slit to the window just before the detector was evacuated to reduce the background scattering from air. The SAXS measurements were performed using two sample-to-detector distances of 0.4 and 1.7 m to cover wider q range, where q is the magnitude of the scattering vector. The scattering patterns were reduced using our original program worked in Igor Pro (WaveMetrics).

RESULTS: Fig. 1 shows the SAXS profiles of the Cu-Ni-Si alloys before and after aging heat treatment. The scattering intensity of the aged sample increases and has a shoulder compared to that of the sample before aging. This contribution is the scattering of the Ni-Si nanoparticles. Because of the recent improvement of the SAXS instrument, the q minimum of the profiles was extended from 0.14 nm^{-1} to about 0.07 nm^{-1}. The present results clearly show that the improvement is beneficial to cover whole the q range of the scattering of the Ni-Si nanoparticles. We will proceed the analysis of size and amount of the Ni-Si nanoparticles.

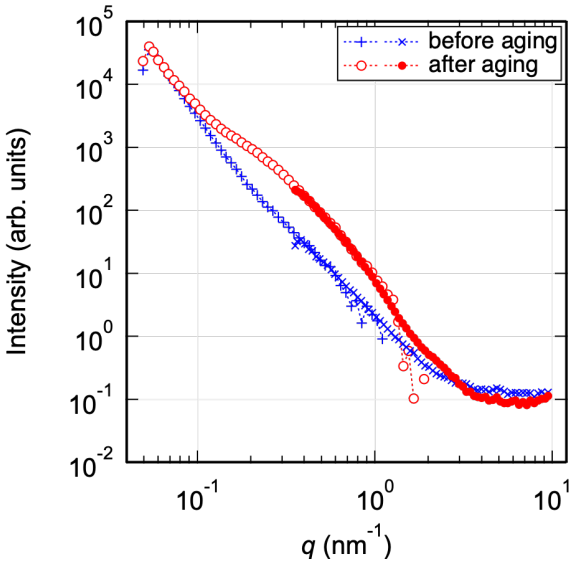

Fig. 1. SAXS profiles of Cu-Ni-Si alloys. Crosses and circles indicate the alloys before and after aging heat treatment, respectively.

REFERENCES:

[1] H. Sasaki et al., Mater. Trans., 63 (2022) 1384-1389.
[2] T. Saito, et al., J. Alloys Compd., 983 (2024) 173852.
[3] Y. Oba, et al., KURNS Prog. Rep. 2024, (2025) 120.

CO4-3

Electrochemical reduction of Fe-containing spinel electrodes for lithium-ion secondary batteries

T. Wada, Y. Arachi
Department of Chemistry, Materials Engineering, Kansai University

INTRODUCTION: In recent years, lithium-ion secondary batteries expand to a wide range of applications, from portable electric appliances to automotive batteries. Spinel-type $Li_4Ti_5O_{12}$ has been practically used as a strain-free insertion negative electrode material. This material exhibits three-dimensional Li-ion diffusion through vacant sites in its structure, suppressing the formation of SEI (solid electrolyte interface) films on the electrode that increase electrical resistance. Therefore, we have focused on a similar structure and examined $LiFeTiO_4$ (LFTO), which operates at approximately 2 V against Li metal. Previous research has shown that LFTO has an inverse spinel-type structure with an ion-distribution of $[Li_{0.5}Fe^{3+}{}_{0.5}]^{8a}[Li_{0.25}Fe^{3+}{}_{0.25}Ti^{4+}{}_{0.5}]_2{}^{16d}O_4$[1]. Furthermore, a significant decrease in discharge capacity has been observed from the first to the second cycle in liquid-type Li-ion secondary batteries using LFTO. However, the reason remains unclear. Therefore, LFTO was prepared under different sintering conditions, and the relationship between the crystal structure of LFTO and its electrochemical properties was investigated from the changes in crystal structure under each charge-discharge state.

EXPERIMENTS: The sample was prepared by conventional solid-state reaction. As starting materials, Li_2CO_3, Fe_2O_3 and TiO_2(anatase) were used and mixed by ball-milling for 30 min at 400 rpm and followed with sintering at 1000 K for 12 h and 1273 K for 6 h in air. The obtained samples were charactered by powder X-ray diffraction and electrochemical testing. As anode and electrolyte, the lithium metal and 1 M $LiPF_6$ in EC-DMC (3:7) were used respectively.

RESULTS: Mössbauer spectroscopy was performed to determine the oxidation state of Fe in LFTO (1273K for 6h) (Fig. 1). Oxidation states and coordination numbers were obtained from isomer shifts (IS) and quadrupole splitting (QS) by fitting for three different Fe components. The results showed that approximately 70% were trivalent in the octahedrons, and the remainder were divalent, occupying roughly equal proportions in the tetrahedrons and octahedra. The presence of some Fe^{2+} suggests the formation of oxygen vacancies. It is also possible that all Fe^{3+} in the tetrahedrons were reduced to Fe^{2+} during sintering and some moved from the tetrahedron to the octahedron sites.

The initial discharge capacity was 68% of the theoretical capacity, which corresponds to the amount of all Fe^{3+} reduced to Fe^{2+} by discharge. On the other hand, the LFTO at 1073 K for 12 h showed an initial discharge capacity was 58% of the theoretical capacity. Rietveld analysis showed the Fe occupancy in the tetrahedron of the former was 0.542(2), while that of the latter was 0.520(2), showing a slight difference in the Fe occupancy in the tetrahedron, and it was found that the high sintering temperature resulted in a 2% higher occupancy compared to the low one. Therefore, it was revealed that while all Fe^{3+} contributes to discharge, slight differences in Fe occupancy within the tetrahedron result in different electrochemical properties.

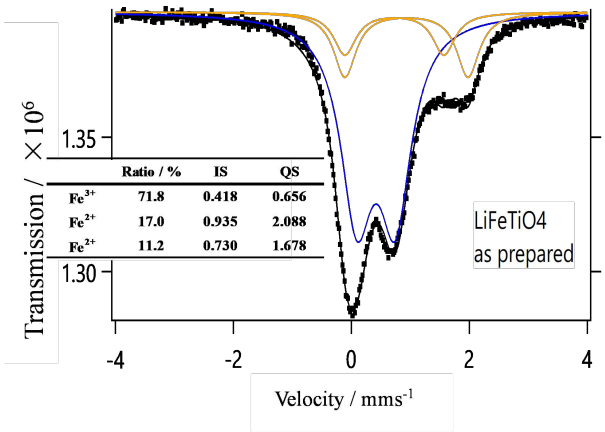

Fig. 1 Mössbauer spectrum of $LiFeTiO_4$ at 300 K prepared by sintering at 1273 K for 6 h.

REFERENCES:

[1] Y. Arachi *et al.*, *J. Jpn. Soc. Powder Powder Metallurg*, **48**(3), 274-276(2001).
[2] Y. Sakai, K. Ariyoshi and T. Ohzuku, *Hyperfine Interactions*, **139/140**, 67-76(2002).

CO4-4

Effects of lead addition on tritium retention behavior in advanced fusion materials

Y. Oya[1], Y. Hoshino[1], S. Okumura[1], Z. Zhang[2], Q. Zhou[2]

[1]*Graduate School of Integrated Science and Technology, Shizuoka University*
[2]*School of Materials Science and Engineering, Wuhan University of Technology*

INTRODUCTION: Tritium will be produced by (n, α) reaction with lithium (Li) in the fusion reactor because the amount of tritium in nature is limited. Tritium breeder requires good chemical stability and ease of tritium recovery. Lithium silicate (Li_4SiO_4) has good chemical stability and good crushing load. Advanced tritium breeder materials should have both of higher tritium production rate and recovery efficiency. Lead (Pb) is a neutron multiplier and has lower affinity with tritium that contributes to the improvement of the tritium breeding ratio. The addition of Pb into Li ceramics is expected to have a potential advantage for the establishment of efficient tritium recovery system.

EXPERIMENTS: LSO-x wt.%Pb, was prepared at Wuhan University of Technology. Those samples were irradiated by neutron at Kyoto University Research Reactor (KUR) with the neutron fluence of 8.0×10^{15} n cm^{-2} and 8.0×10^{16} n cm^{-2} (1MW 4h and 5MW 1h). After the neutron irradiation, tritium release behavior was evaluated by Tritium-thermal desorption spectroscopy (T-TDS) system by heating the samples separately from R.T. to 1113 K with the heating rates of 10, 20, and 30 K min^{-1}. In T–TDS, HT was oxidized to HTO using copper oxide, and all tritium species released by heating, including HT and HTO, were captured in a water bubbler. Liquid scintillation counter (LSC) was used to measure the total T amount trapped by the water bubbler at Shizuoka University.

RESULTS: Fig. 1 show the HTO and HT desorption rates of pure LSO at heating rate of 10 K /min, 20 K/min and 30 K/min. Fig. 2 show the HTO and HT desorption rate of LSO-10 wt.%Pb, heating rate are 10 K/min, 20 K /min and 30 K/min. The desorption peak of HTO consisted of a single peak, whereas three peaks were observed for HT at around 400 K, 600 K, and 800 K. These differences were considered to be caused by variations in the trapping sites. Also, it was observed that as the heating rate increases, the peak temperature was shifted toward the high-temperature side. When compared with the desorption peaks of pure Li_4SiO_4 ceramics, the present desorption peak was markedly shifted to a lower temperature, which lead to conclude that lead addition improve the efficient tritium reconvery at lower temperature.

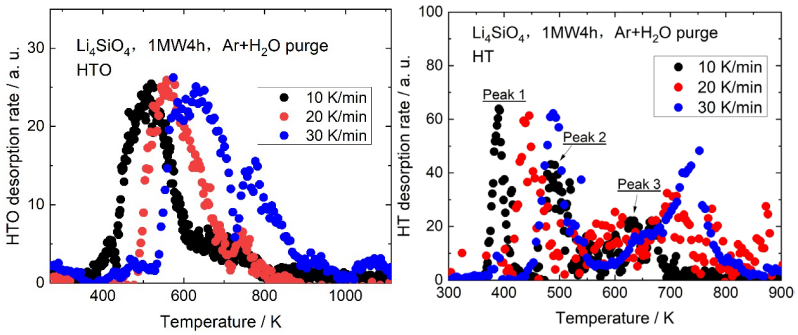

Fig.1 T-TDS spectra of Li_4SiO_4 (Left: HTO, Right: HT)

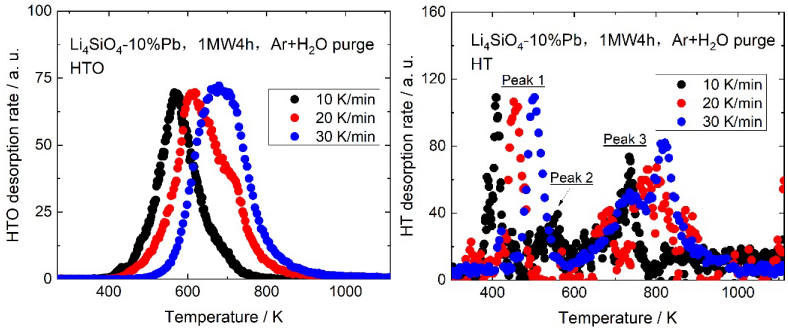

Fig.2 T-TDS spectra of Li_4SiO_4-10%Pb (Left: HTO, Right: HT)

CO4-5

Point defect and impurity effect on mechanical property and irradiation damage evolution in $Cr_{0.8}FeMn_xNi_y$ concentrated solid solution alloy

N. Hashimoto[1], S. Sudo[2], K. Fukumoto[2], H. Oka[1], S. Isobe[1]

[1] *Div. of Materials Science and Engineering, Faculty of Engineering, Hokkaido Univ.*
[2] *Div. of Materials Science and Engineering, Graduation School of Engineering, Hokkaido Univ.*

INTRODUCTION: It has been reported that some concentrated solid solution alloys (CSAs) and high entropy alloys (HEAs) have unique properties such as a high radiation resistance and corrosion resistance at elevated temperatures compared with conventional nuclear component materials [1-2]. This attractive property could make CSAs and HEAs candidates for high temperature nuclear reactor components. In this study, we focused on microstructure and mechanical property in FCC-type CSAs and an HEA in order to better understand the effect of point defect and impurity on mechanical property and irradiation damage evolution.

EXPERIMENTS: The materials used in this study are FCC-type single phase $Cr_{0.8}FeNi_xMn_y$ alloys, prepared by arc-melting or induction furnace in high-purity argon atmosphere, followed by solution annealing at 1160 °C for 24 hrs. For the estimation of the stacking fault energy (SFE), samples were cold-rolled down to 0.25 mm in thick, then punched out for tensile test. The in-situ irradiation experiment was performed using the multi-beam High Voltage Electron Microscope at Hokkaido University. All the TEM samples were electron-irradiated at 500 °C up to 1 dpa.

RESULTS: The estimated SFE values from 5%-deformed $Cr_{0.8}FeNi_xMn_y$ alloys seemed to increase as a function of Ni and Mn concentration. In addition, the tensile test revealed that the yield strength, the elongation, and even hardening rate were increased with increasing Ni and Mn concentration. Furthermore, $Cr_{0.8}FeNi_xMn_y$ alloys including high C and N indicated a higher yield strength and a longer elongation compared to the high purity $Cr_{0.8}FeNi_xMn_y$ alloys. Electron irradiation experiment at 400°C showed the formation ofblack dots and frank loops (FLs), but no cavities in $Cr_{0.8}FeNi_xMn_y$ alloys (Fig. 1). The decrease in FL number density with increasing Ni and Mn concentration was observed, but no obvious relationship with loop size. Furthermore, $Cr_{0.8}FeNi_xMn_y$ alloys including high C and N tended to have a higher FL number density and smaller size.

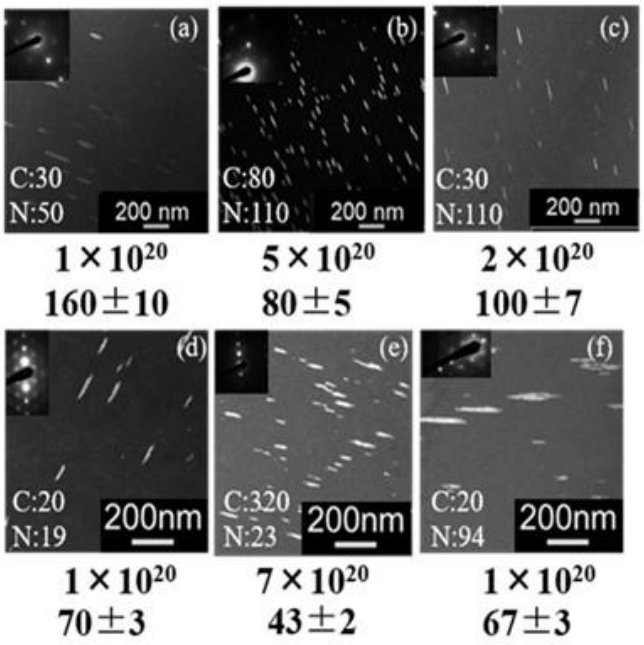

Fig.1 Dark field relrod image of Cantor alloys (a-c) and $Cr_{0.8}FeMnNi$ alloys (d-f) electron-irradiated at 400 °C to 0.2 dpa. Impurity concentration (wppm) is shown in the lower left corner. Loop number density (m^{-3}) is shown in the first line at the bottom outside the image, and mean loop diameter (nm) is shown in the second line.

REFERENCES:

[1] S.J. Zinkle and L.L. Snead, Annu. Rev. Mater. Res. 44 (2014) 241-267.

[2] M.H. Tsai and J.W. Yeh, Mater. Res. Lett. 2 (2014) 107–123.

CO4-6

Controlled Interfacial Polymerization Polyamide/Polysulfone Membrane Probed by Slow Positron Beam

Z. Chen [1], Y. Kobayashi [2] A. Yabuuchi[3] and A. Kinomura [3]

[1] *Department of Material Science and Engineering, Wuhan Institute of Technology, People's Republic of China*

[2] *Department of Environmental Science, Tokyo Gakugei University*

[3] *Institute for Integrated Radiation and Nuclear Science, Kyoto University*

INTRODUCTION: Polyamide/Polysulfone nanofiltration membranes have been widely used in water treatments due to their high efficiency, low energy consumption [1]. The surface charge, pore size and its distribution in the polyamide layer play an important role in membrane selectivity. A more uniform polyamide layer might be prepared by controlling the interfacial polymerization reaction rate[2]. In this study, TMC/hexane solution was slowly added to the piperazine (PIP) solution through a controlled injection. And the obtained composite membranes have been investigated via positron annihilation techniques coupled with a positron beam.

EXPERIMENTS: 10 ml PIP aqueous solution was dropped onto the PES substrate. Then 5 ml pure hexane was added. After 1 min, TMC/hexane solution was added to the pure hexane with an injection pump at a constant speed. The total releasing and reaction time of TMC solution was 2 min, 3 min, 4 min and 5 min, respectively. The prepared samples were named as IP-2, IP-3, IP-4 and IP-5, respectively. Positron measurements were performed with the position beam system at the Institute for Integrated Radiation and Nuclear Science, Kyoto University.

RESULTS: As shown in Fig. 1, the *S-E* curves of the four membranes reveal the differences in their layer structures, despite exhibiting a similar shape. The difference in *S* parameters in the low incident energies suggests structural differences within the polyamide layers. Moreover, the results of the o-Ps lifetimes and the molecular weights of polyamide by GPC are presented in Table 1. It is interesting to find that the decrease in the reaction rate leads to a smaller free-volume hole size (shorter o-Ps lifetime) and lower Mw/Mn, suggesting that longer injection time should lead to a narrower distribution of molecular weight. Since the injection rate was the sole variable in the preparation process, the reaction rate would be responsible for the different structures of the polyamide layers. These findings suggest that controlling monomer release rates could promote more uniform and complete crosslinking reactions.

Table 1 The o-Ps lifetime and molecular weight of polyamide

	o-Ps lifetime [ns]	o-Ps intensity[%]	Mn	Mw	Mw/Mn
IP-2	1.60	23.5	12945	3292	79.7
IP-3	1.54	28.7	12705	4117	75.5
IP-4	1.51	30.0	12024	1930	52.0
IP-5	1.27	26.4	10060	7892	56.0

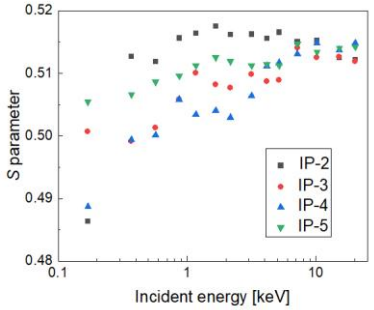

Fig. 1 *S-E* plots of the samples

REFERENCES:

[1] Y. Cui *et al.*, Water Research, **200** (2021) 117207.

[2] J. Hu *et al.*, Journal of Membrane Science, **720**(2025) 123773

CO4-7

Complex Structure of Ions Coordinated with Hydrophilic Polymer 26. "Diffusion-induced Orientation" Observed in PA6 and Amphiphilicity in Iodine-doped Polymers Considering Dynamic Behavior of Polyiodides.

A. Kawaguchi[1], A. Kita[1], Y. Morimoto[1]

[1] *Institute for Integrated Radiation and Nuclear Science, Kyoto University*

INTRODUCTION: At first, interacted structuring between polyamide 6 (PA6, Nylon^{TM}-6) and iodine (polyiodides, I_n^{m-}, "PolyIod" as below) had been considered in discussion of structural transition of PA6 crystal (α-phase) or conversion of hydrogen bonding in PA6 crystallites.[1] However, while preparation of the samples is not so difficult and WAXD patterns are also observed explicitly, structure analysis and quantitative reproduction have not been concluded even in half century after the first report.

One of characteristic and unexpected behaviors observed in "iodine-doping" for PA6 is "diffusion-induced orientation" which is considerably unique as modification of orientation in mesoscopic scale achieved (almost) simultaneously with rapid ionic diffusion and coordination in PA6 crystallite; "diffusion-induced orientation" is almost simultaneously observed both in SAXS range of X-ray diffraction and in WAXD for crystallite structure.[2]

And, additionally, iodine-coordinated ("iodine-doped") structures are activated and/or modified by environment (ionic diffusion responding with humidity, modified abnormal intercalation,, etc.) not only during initial diffusion of "PolyIod" into PA6 matrix but also after "iodine-doping"; easy ionic exchange activated in iodine-doped PA6 or other matrices is applied for hybrid nano-composite without synthesis nor melting nor casting for matrices.

RESULTS AND DISCUSSION: The author regards that lots of unconscious factors complicate results and that interaction invisible as chemical structure of "PolyIod" molecules plays intrinsic roles on all behavior through nano and mesoscopic scales. For example, utilizing activated ionic diffusion deeply through "iodine-doped" PA6 matrix and ionic exchange *a posteriori* ("secondary doping" of inorganic salts as nano filler or "as shaped" hybrid composite).

Arguing PA6, "diffusion-induced orientation" observed on "(1st) iodine doping" to PA6 matrix may be a singular case depending on relation between lattice constants (symmetry) provided by PA6 α-crystallite and "PolyIod".[3] However, rapid diffusion and modified orientation suggest self organization provided by "iodine bonding" and dynamics (coupling and decoupling) between "PolyIod"'s under anisotropic coordination layout.

These results suggest *dynamic interaction and structures* for both (guest) "PolyIod" and (host) polymer matrices.[4] While direct experimental observation of suggested models may not be easy, such hypothesized views can reasonably explain unexpected experimental issues previously reported.

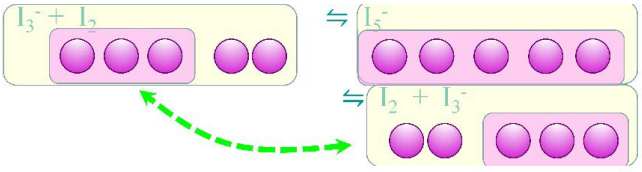

Fig. 1. example of dynamic coupling and decoupling (linear) models between "PolyIod" to explain amphiphilicity and "diffusion-induced orientation"; linear or L-shaped self coordination between "PolyIod" is induced by "iodine bonds" as halogen bonding or "σ-hole".

REFERENCES:

[1] H. Arimoto, Kobunshi Kagaku, **19** (1962) 456-460.
[2] A. Kawaguchi *et al.*, Polym. Prep. Jpn., **50** (2001) 2000-2000.
[3] K. Tashiro *et al.*, Polym. J., **58** (2026) 137-148.
[4] A. Kawaguchi, Polym. Prep. Jpn., **67** (2018) [presentation "2I-18"].

CO4-8

Correlation between the spin-relaxation of ^{111}Cd(←^{111}In) in glycerin solution and its viscosity

M. Tanigaki[1], S. Ijichi[2], K. Matsuta[1], A. Taniguchi[1], and Y. Ohkubo[1]

[1] *Institute for Integrated Radiation and Nuclear Science, Kyoto University*
[2] *Graduate School of Science, Kyoto University*

INTRODUCTION: Quasi-droplets, extremely tiny water droplets as small as 1/10,000th the thickness of a human hair, show various functions differently from normal water [1], but the exact mechanism behind their functions or even the basic properties, such as internal pressure, pH, and viscosity, are still unknown because of their smallness. Radioactive nuclei can be a good probe for such extremely small substances [2]. Steffen demonstrated the applicability of radioactive nuclei to the measurement of viscosity [3]. Still, their result is unreliable due to insufficient time resolution and limited knowledge of the ion status in the solvent. This time, we studied the correlation between the viscosity and the spin relaxation of ^{111}Cd(←^{111}In) using time differential perturbed angular correlation (TDPAC) at higher time resolution and under controlled conditions, intending the application to the studies of quasi-droplets.

EXPERIMENTS: Typical four-counter TDPAC measurements were performed for the 171-245 keV cascade in ^{111}Cd(←^{111}In) in the samples of glycerin aqueous solution of viscosity η within the range of 0.5~4000 mPa·s. The viscosity of each sample was controlled by changing its temperature and density. The pH of each sample was maintained below 3 by adding dilute HCl_3 to eliminate the possible interference to the spin relaxation pattern caused by the multiple formation of ligand at the intermediate pH [4].

RESULTS AND DISCUSSION: Observed $G_{22}(t)$ spectra consist of two components, a fast relaxation caused by the after-effect and a slow relaxation after 60 ns. The slow component was dominant at lower viscosities up to several tens mPa·s, while the fast component was dominant at higher viscosities. A simple exponential function was applied to the slow component of each $G_{22}(t)$ to evaluate the decay constant of spin relaxation, λ. Even though the obtained values of λ were ten times smaller than those reported by Steffen, they were consistent with the models of lower η proposed by Abragam [5] and higher η by Marshall [6]. The correlation between λ (sec^{-1}) and η (mPa·sec) can be expressed in a simple function (Fig.1):

$$\lambda = \frac{2.4 \times 10^5 \eta}{1 + 1.3 \times 10^{-3} \eta^2}$$

With the present result, we expect that the viscosity of quasi-droplets can be determined by the TDPAC method once a method of introducing ^{111}In to the quasi-droplets is developed.

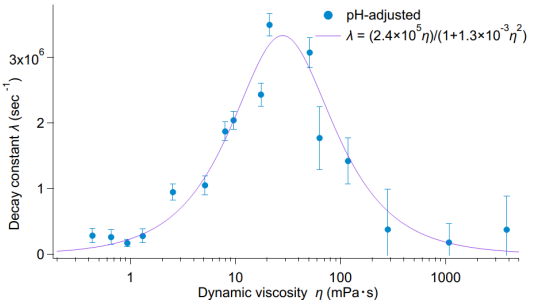

Fig. 1. Correlation between the decay constant of spin relaxation and the viscosity of the solution.

REFERENCES:

[1] Y. Tamura, et al. J. Bacteriol, **206**, e00139-24 (2024).
[2] M. Tanigaki et al., Chem. Eng. Technol. **46,** 1773 (2023).
[3] R. M. Steffen, Phys. Rev. **103**, 116 (1956).
[4] G. R. Demille et al., Chem. Phys. Lett. **44**, 164 (1976).
[5] A. Abragam and R. V. Pound, Phys. Rev. **92**, 943 (1953).
[6] A. G. Marshall and C. F. Meares, J. Chem. Phys. **56**, 1226 (1972).

CO4-9

Deformation of Local Structures in Hafnium Metal Induced by Hydrogen Absorption

W. Sato[1,2], S. Katayama[2], Y. Shimizu[2], H. Shimizu[2] and A. Taniguchi[3]

[1] *Institute of Science and Engineering, Kanazawa University*
[2] *Graduate School of Natural Science and Technology, Kanazawa University*
[3] *Institute for Integrated Radiation and Nuclear Science, Kyoto University*

INTRODUCTION: Hafnium (Hf) metal is a well-known material as a control rod in a nuclear reactor due to the large neutron-capture cross sections of some of the isotopes. Because the control rods are exposed in high-temperature and high-pressure cooling water for a long period, however, hydrogen atoms arising from the coolant are absorbed into the lattice of the metal, which causes the formation of lattice defects leading to the embrittlement of the material such as a cracking of a cladding tube for the control rods. In order to prevent nuclear accident, it is important to understand the characteristics of the hydrogen-induced lattice defects as well as the thermal behavior of hydrogen impurities themselves in Hf. In the present work, we have tried to observe the effect of hydrogen absorption on the local structures using two different nuclear spectroscopic techniques: perturbed angular correlation (PAC) spectroscopy with the ^{181}Hf(→^{181}Ta) probe and positron annihilation lifetime spectroscopy (PALS). Here, we report preliminary results on the effect of hydrogen absorption into the lattice of Hf matrix.

EXPERIMENTS: A Hf metal plate (5×5×0.5 mm^3) of a purity of about 96.4% with 3.6% Zr impurity was irradiated with thermal neutrons in the research reactor of Kyoto University (KUR) to produce the ^{181}Hf(→^{181}Ta) probe, and TDPAC measurements were performed by detecting the 133-482 keV cascade γ rays with the intermediate level of I = 5/2 having a half life of 10.8 ns. Apart from the PAC experiment, PALS measurements were performed for a pristine and hydrogen-absorbed Hf plates at room temperature using a positron source of ^{22}Na. The PALS spectra were analyzed with a fitting program PALSfit [1]. For the absorption of hydrogen atoms into Hf lattice, we adopted an electrolytic reaction of water in 0.5 M H_2SO_4 aqueous solution by applying a constant current of 1.5 Acm^{-2} for 90 min to a Hf plate as the cathode. The detail of the electrolysis is described in Ref. [2].

RESULTS: PALS measurements disclosed the effect of hydrogen absorption on the local structure in the Hf lattice, demonstrating enlargement of vacancy clusters, which signifies the change in the local structure of the lattice. As shown in Fig. 1, PAC measurements reveal that the probe occupies only a single site in the pristine Hf metal, but another component was observed in the PAC spectrum for the hydrogen-absorbed Hf, showing local deformation by hydrogen insertion. Both the results of spectroscopies are consistent. For further discussion on the hydrogen effect, detailed analyses are underway.

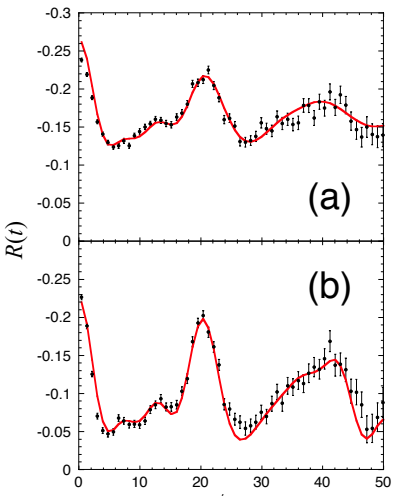

Fig. 1. PAC spectra of the ^{181}Hf(→^{181}Ta) probe (a) in a pristine and (b) in a hydrogen-absorbed Hf plate.

REFERENCES:

[1] J. V. Olsen, P. Kirkegaard, N. J. Pedersen and M. Eldrup, Phys. Status Solidi C **4** (2007) 4004-4006.
[2] W. Sato, M. Furumoto, H. Shimizu and Y. Ohkubo, J. Appl. Phys. **135** (2024) 245103/1-6.

CO4-10

Study on ^{99m}TcSeparation/Concentration Technology from ^{99}Mo by (n, γ) Method (4)

H. Suematsu[1], Y. Yang[1], H. Ito[1], A. V. Le[1], Y. Su[1], S. Kato[1], T. M. D. Do[1], T. Suzuki[1], N. Osawa[1], Y. Fujita[2], Y. Fujihara[3], H. Yoshinaga[3] and J. Hori[3],

[1] *Graduate School of Engineering, Nagaoka University of Technology*
[2] *Fuels and Materials Department, Japan Atomic Energy Agency*
[3] *Institute for Integrated Radiation and Nuclear Science, Kyoto University*

INTRODUCTION: Previous studies have demonstrated the successful recovery of recoil "hot atoms" from irradiated β-MoO_3 targets, indicating that the extraction efficiency of ^{99}Mo increases continuously over time [1]. A key objective of the present study is to evaluate the recyclability of the target material following the aqueous extraction process. To investigate this, β-MoO_3 powder from previous experiments which had been previously immersed in water for extraction and subsequently dried, was re-irradiated to assess its ^{99}Mo production capacity and structural stability. Furthermore, this research expands the scope of investigation to evaluate the extraction efficiencies of alternative molybdenum oxides, such as Mo_4O_{11}.

EXPERIMENTS: The hydrated sample was prepared by immersing β-MoO_3 in water at 80°C for 12 hours. The dehydrated counterpart was subsequently obtained by calcining the hydrated material in a furnace at 280°C for 2 hours. For comparison, Mo_4O_{11} was synthesized from MoO_2 under an argon atmosphere at 600°C for a duration of three days.
All samples were irradiated at the Kyoto University Reactor (KUR) with a thermal neutron flux of 3×10^{13} n cm^{-2} s^{-1} for 20 minutes; these parameters were selected to remain consistent with established irradiation conditions from previous studies [1]. Following irradiation, the powders were dispersed in distilled water and stirred for 5.5 hours at room temperature to facilitate the aqueous extraction of the recoil atoms. The final extraction yield of ^{99}Mo was determined by quantifying the induced radioactivity via gamma-ray spectrometry using a high-purity germanium (HPGe) detector.

RESULTS: The ^{99}Mo extraction efficiencies for the various molybdenum oxide samples are illustrated in Fig. 1. Among the tested materials, the dehydrated β-MoO_3 exhibited the highest extraction rate. In contrast, the hydrated sample showed a significantly lower extraction efficiency compared to the pristine β-MoO_3 phase. This suggests that the presence of lattice-bound water may serve as a barrier, inhibiting the migration of ^{99}Mo recoil atoms from the crystalline bulk to the grain surfaces. Measurements of commercial MoO_2 yielded low extraction values, consistent with previously reported data [2]. Moreover, the Mo_4O_{11} synthesized from the commercial MoO_2 precursor demonstrated negligible ^{99}Mo recovery. These results provide further evidence that the specific crystalline structure and oxidation state of molybdenum oxides are decisive factors in governing the mobility and subsequent aqueous extraction of hot atoms.

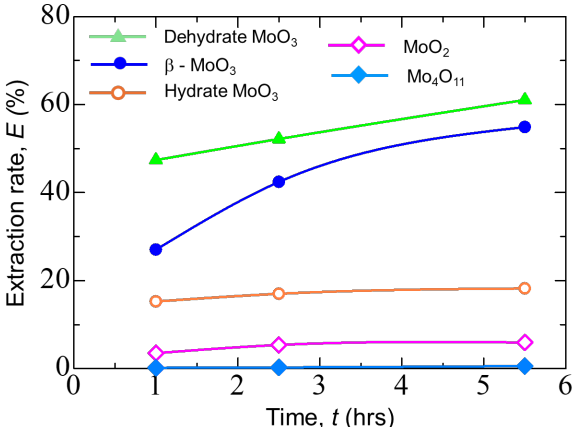

Fig.1 Extraction rate of ^{99}Mo compounds

REFERENCES:
[1] M. C. Chu *et al.*, Inorganic Chem., **62** (2023) 131040.
[2] X. Hu *et al.*, J. Radioanal. Nucl. Chem., **333** (2024) 6057–6063.

CO4-11

Investigation of Cd Occupation Sites in $SrTi_{1-x}Cd_xO_3$ by TDPAC Measurements

S. Komatsuda[1], W. Sato[2], A. Taniguchi[3], M. Tanigaki[3], and Y. Ohkubo[3]

[1]*Institute of Human and Social Sciences, Kanazawa University*
[2]*Institute of Science and Engineering, Kanazawa University*
[3]*Institute for Integrated Radiation and Nuclear Science, Kyoto University*

INTRODUCTION: $SrTiO_3$ is one of the most promising candidates for photocatalytic materials. Trivalent cation doping at the Ti^{4+} site is known to be an effective approach for improving photocatalytic activity. Our previous study demonstrated that the addition of Cd in $SrTi_{1-x}Cd_xO_3$ enhances photocatalytic activity, which reaches a maximum at a Cd concentration of 4% and declines at higher concentrations. In addition, XRD measurements on $SrTi_{1-x}Cd_xO_3$ revealed a systematic increase in the lattice parameter with increasing Cd content, suggesting that Cd occupies the Ti site in the perovskite lattice. For the practical use of $SrCd_xTi_{1-x}O_3$, it is necessary to obtain microscopic information on impurity sites. Therefore, for the study of the local fields at Cd sites, the TDPAC measurements were performed for ^{111}Cd(←^{111m}Cd) in $SrTi_{1-x}Cd_xO_3$ (x=0.01, 0.02, 0.03, 0.04, 0.05).

EXPERIMENTS: Stoichiometric amount of $SrCO_3$, $CdCO_3$, and TiO_2 powders was mixed in a mortar. The powders were pressed into disks. For TDPAC measurements, about 3 mg of CdO enriched with ^{110}Cd was irradiated with thermal neutrons at Kyoto University Research Reactor, and radioactive ^{111m}Cd was generated by the ^{110}Cd(n, γ)^{111m}Cd reaction. The neutron-irradiated CdO powder was dissolved in 6M HCl and added in droplets onto the pre-sintered $SrTi_{1-x}Cd_xO_3$ disk. The disk was sintered in air at 1373 K for 90 min. TDPAC measurements were carried out for the 151-245 keV cascade γ rays of ^{111}Cd(←^{111m}Cd) probe with the intermediate state of I = 5/2 having a half-life of 85.0 ns.

RESULTS: Figure 1 shows one of the TDPAC spectra of the ^{111}Cd(← ^{111m}Cd) probe in $SrTi_{1-x}Cd_xO_3$ (x=0.02) at room temperature. The TDPAC spectrum was successfully reproduced by a two-component fit. From the fitting parameters, the first component exhibited a quadrupole frequency of ω_Q = 23.2 Mrad/s, a fractional intensity of f = 83%, and a Gaussian frequency distribution of δ = 77%, while the second component showed a quadrupole frequency of ω_Q = 49.3 Mrad/s, a fractional intensity of 12%, and Gaussian distribution of δ = 0%. For the first component, the large distribution suggests that these Cd atoms reside at disordered lattice sites. In contrast, the second component exhibits no frequency distribution, indicating that Cd occupies a well-defined lattice site. The quadrupole frequency of this component is close to the value of 50.6 Mrad/s previously reported for ^{111}In at the Ti site in $SrTiO_3$ [1], suggesting that this component may originate from Cd substituting for Ti in the $SrTiO_3$ lattice. These results suggest that Cd partially occupies the Ti site in $SrTiO_3$ and may contribute to the enhanced photocatalytic activity.

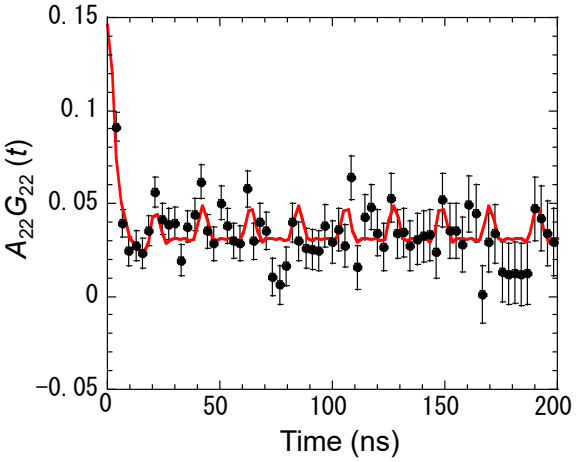

Fig. 1. TDPAC spectrum of ^{111}Cd(←^{111m}Cd) in $SrCd_{0.02}Ti_{0.98}O_3$ at room temperature.

REFERENCE:

[1] S. Komatsuda *et al.*, Interactions, **245** (2024) 37.

CO4-12

Observation of Waveform of Wien Bridge Oscillator under Irradiation of Bremsstrahlung x-ray Produced by Pulsed Electron Beam

Y. Gotoh[1], A. Kinomura[2], and T. Takahashi[2]

[1] *Graduate School of Engineering, Kyoto University*
[2] *Institute for Integrated Radiation and Nuclear Science, Kyoto University*

INTRODUCTION: Field emitter arrays (FEAs) fabricated by contemporary thin-film and micro-fabrication technologies are expected to be used in harsh environments such as radiation fields, and several electronic devices were developed so far for this purpose [1-4]. It is important to confirm stable operation of the electronic circuits in radiation fields. Use of pulsed electron beam to produce pulsed x-ray is a good method to observe the response of the electronic circuit due to radiation. In this report, results of preliminary experiments to confirm the operation of an oscillator under radiation field are described.

EXPERIMENTS: In prior to experiments with FEAs, preliminary experiments were performed with a solid-state electronic circuit instead of vacuum devices. Two junction-type field effect transistors were used. Wien bridge oscillator of which oscillation frequency was approximately 100 kHz was prepared. The oscillator was installed in a capsule made of stainless steel. A battery was used to operate the oscillator. The sample was irradiated by Bremsstrahlung x-ray produced in platinum target under irradiation of 6 MeV pulsed electron beam with a pulse width of 4 μs and repetition frequency of 1 to 100 Hz. The output of the oscillator was monitored with an oscilloscope via 15 m-long coaxial cable. To reduce the effect of the capacity of the cable, a large resistor was inserted, which reduced the amplitude of the observed signal.

RESULTS: Figure 1 shows a typical wave form of the oscillator. The x-ray was irradiated between -4 and 0 μs. When the x-ray was irradiated on the sample, the amplitude of the oscillation signal was once reduced, and then recovered. However, such behavior was observed even when the oscillator was moved to the location apart from the target. When the cable that supplies the electric power from the battery was shortened, the reduction of the amplitude was not observed, as shown in Fig. 2. This response was found to be attributed not to the effect of x-ray on the circuit, but rather to that on the battery. From these results, it was suggested that the amplitude of the oscillator was affected by the electric signal which was generated by the accelerator power supply. Further investigation with an improved shielding will be necessary.

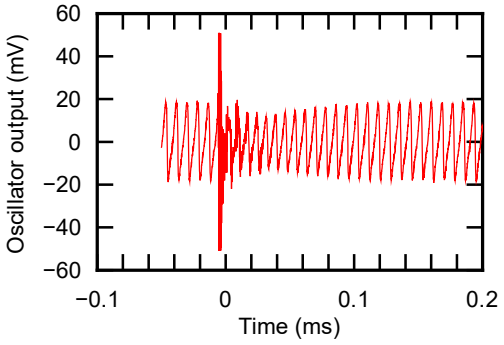

Fig. 1. Wave form of the oscillator under x-ray irradiation.

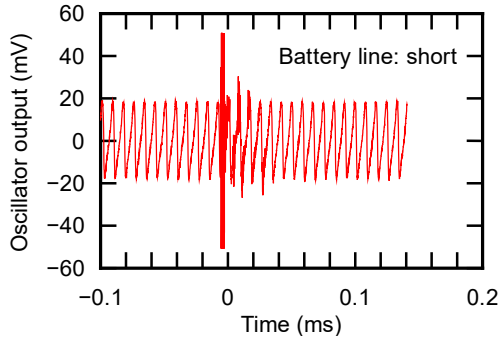

Fig. 2. Wave form of the oscillator with a shortened battery line.

REFERENCES:

[1] K. Ikeda *et al.*, J. Vac. Sci. Technol. B **29** (2011) 02B116.
[2] Y. Gotoh *et al.*, J. Vac. Sci. Technol. B **31** (2013) 050601.
[3] R. Hori *et al.*, J. Vac. Sci. Technol. B **43** (2025) 043201.
[4] Y. Gotoh *et al.*, IEEE Trans. on ED **67** (2020) 1660.

Evaluation of neutron shielding properties and radioactivation of wood and wood composites.

K. Murata[1], Y. Mimoto[1], M. Tsuchiya[2], K. Kariya[2], Y. Yamashiki[3], K. Takamiya[4]

[1]*Graduate School of Agriculture, Kyoto University*
[2]*Sumitomo Forestry Co., Ltd.*
[3]*Graduate School of Advanced Integrated Studies in Human Survivability, Kyoto University*
[4]*Institute for Integrated Radiation and Nuclear Science, Kyoto University*

INTRODUCTION: Neutron shielding is typically achieved using hydrogen-rich materials such as water, polyethylene, and concrete, while boron is commonly used as a neutron absorber due to its large absorption cross-section. Because wood is mainly composed of carbon, oxygen, and hydrogen, wood-based materials can exhibit good neutron shielding performance. In this study, we developed wooden shielding material and evaluated the variability in shielding performance and gamma-ray dose during irradiation at the Heavy Water Neutron Irradiation Facility (HWNIF) in KUR.

EXPERIMENTS: Table 1 shows the materials prepared for neutron shielding test, which have a cross section of 90 × 90 mm and a thickness of 60 mm. Three Au foils were placed in front of and behind the specimen at the upper, middle, and lower positions along the specimen height. These specimens were irradiated with mixed-mode neutron radiation in the HWNIF for 10 min. Gamma rays from the activated Au foils were measured using a high-purity germanium detector, and shielding rates were obtained. Furthermore, the gamma-ray dose behind the specimen during irradiation was measured using a thermoluminescence dosimeter.

RESULTS: Fig. 1 shows the neutron shielding rates measured at different positions. Uniform shielding performance was observed in WS, a mixture of wood and boron, and its shielding rate was comparable to that of PE. This result indicates that WS can provide stable neutron shielding performance comparable to that of conventional shielding materials. Table 2 compares the gamma-ray dose emitted from the specimens. The gamma-ray dose emitted from SG was lower than that from PE. In contrast, WS showed the highest dose due to the 0.478 MeV gamma rays produced via the $^{10}B(n,\alpha)^{7}Li$ reaction. These results suggest that although WS demonstrates favorable neutron shielding capability, additional considerations are required regarding the gamma-ray dose generated during neutron irradiation. Future work will focus on optimization material design by considering the trade-off between shielding performance and radioactivation.

Table 1 List of materials used in this study.

Symbol	Material
PE	Polyethylene
SG	Air-dried sugi wood
WS	Wooden shielding material containing boron

Table 2 Gamma-ray dose from the irradiated specimens.

Material	Dose (Gy)
PE	0.108
SG	0.0849
WS	0.181

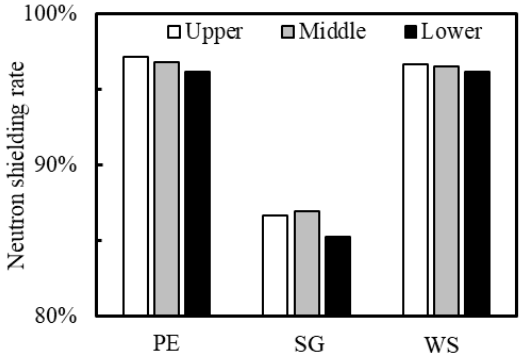

Fig. 1 Neutron shielding rates at given positions along the specimen hight (Upper, Middle. Lower).

CO4-14

Slow Positron Probe Analysis of Fe-Cr Alloy Thin Films Subjected to Severe He Ion Irradiation

Y. Kamada[1], S. Yoshida[1], K. Ito[1] and A. Kinomura[2]

[1] *Faculty of Science and Engineering, Iwate University*
[2] *Institute for Integrated Radiation and Nuclear Science, Kyoto University*

INTRODUCTION: If nuclear fusion reactions can be controlled on Earth, an essentially limitless source of clean energy could be obtained. Currently, the design and construction of experimental and prototype reactors are underway, but numerous challenges remain. In tokamak-type reactors, the "blanket" responsible for energy conversion, is subjected to severe neutron irradiation, which alters various material properties during operation. Focusing on Fe-Cr alloys as candidate materials, their magnetism is directly linked to the electromagnetic forces applied to the reactor structure during plasma disruptions. Therefore, understanding the effects of irradiation on magnetism is essential; however, research has been limited due to experimental difficulties. Neutron irradiation experiments are costly and time-consuming, and the activation of samples requires hot laboratories. Alternatively, ion irradiation offers advantages such as shorter duration and non-activation, but the damage is confined to the surface region, complicating magnetic evaluation. To overcome this challenge, a method using ion irradiation of high-quality alloy thin films has been proposed, and research has progressed. To clarify the effects of nuclear transmutation helium, Fe-Cr alloys were subjected to severe helium irradiation, and their structure and magnetism were investigated, leading to the discovery of high-density cavity formation and magnetic hardening phenomena [1]. The latter was not observed in pure iron [2], suggesting that irradiation-induced changes in the atomic distribution of chromium are key. In this study, to gain further insight into irradiation damage structures, Fe-Cr alloy thin film samples were irradiated with helium ions, and defect evaluation was conducted using a low-energy positron beam.

EXPERIMENTS: Using ultra-high vacuum electron beam evaporation, 300 nm thick Fe-20%Cr films were grown on MgO(001) substrates. Helium ions with an energy of 50 keV were irradiated at room temperature using the microwave ion source at the Wakasa Wan Energy Research Center (WERC). The irradiation dose was set to 1.7×10^{17} ions/cm². Small pieces were cut out from the irradiated samples by FIB processing for cross-sectional TEM observation. Furthermore, Doppler broadening measurements were performed at energies up to 30 keV using the low-energy positron beamline, and the S and W parameters were evaluated.

RESULTS: The fabricated thin film was confirmed to be epitaxially grown with the orientation relationship BCC-Fe-Cr(001)[110]//MgO(001)[100]. In the positron annihilation experiment, the S parameter showed a significant increase in the energy range of 5 to 7 keV due to He ion irradiation. Cross-sectional TEM observations confirmed the formation of a high density of cavities with sizes of a few nanometers, and the increase in the S parameter is considered to reflect these nanoscale structural changes.

ACKNOWLEDEMENT:
This work was partly supported by JSPS KAKENHI Grant Number 24K21745. We would also like to express our gratitude to Dr. Ishigami at WERC for their invaluable support in conducting the irradiation experiments.

REFERENCES:
[1] Y. Kamada *et al.*, Metals, **14** (2024), 568. [2] Y. Kamada *et al.*, Metals, **13** (2023), 1905.

CO4-15

Study on HPLC Elution Behavior of Heavy Lanthanide Metallofullerene

K. Akiyama[1], D. Nakamura[1], T. Kuroda[1], K. Takamiya[2], and S. Kubuki[1]

[1] *Department of Chemistry, Tokyo Metropolitan University*
[2] *Institute for Integrated Radiation and Nuclear Science, Kyoto University*

INTRODUCTION: Lanthanide (Ln) metallofullerene (EMF): Ln@C_{82} is a clathrate compound encapsulating metal atom in fullerene C_{82} and known that two or three electrons are transferred to C_{82} cage from the encapsulated Ln atom [1]. In the previous work, we succeeded to obtain the high-performance liquid chromatography (HPLC) elution behavior on a pyrenyl stationary phase for Ln@C_{82} of La, Ce, Pr, Nd, Gd, Tb, Dy, Ho, and Er with a toluene as an eluent by the thermal neutron activation method [2]. On the other hand, the results obtained by analyzing long half-life nuclides such as Ce and Tb had problems in accuracy compared to other short half-life nuclides. In this study, we attempted to obtain data again for the long half-life nuclides Tb-160 and Ho-166, and at the same time attempted to improve accuracy by conducting HPLC development and analysis.

EXPERIMENTS: Ln@C_{82}s of Tb, Dy, and Ho were prepared by previously reported [2]. These purified samples were injected into a Buckyprep column using toluene as an eluent. The eluent from the column was fractionated every 20 seconds at room temperature (RT) and 40°C, and every 1 minute at 10°C. These fractions were evaporated to dryness, and re-dissolved in CS_2. These CS_2 solutions were dropped and dried on a filter paper with a diameter of 12 mm, and then sealed in a polyethylene bag. These samples were irradiated with thermal neutrons in the KUR of the Institute for Integrated Radiation and Nuclear Science, Kyoto university. After the irradiation, the γ rays emitted from the samples were measured by a Ge detector.

RESULTS: The figure shows HPLC chromatograms of Tb and Ho fullerenes developed on a pyrenyl stationary phase at 40°C, RT, and 10°C. The HPLC retention time of Ln@C_{82} fullerene at each temperature were found to be 45.75±0.02 min. at 40 °C, 55.55±0.02 min. at RT, and 61.22±0.03 min. at 10 °C for Tb@C_{82}, and 45.25±0.02 min. at 40 °C, 54.99±0.03 min. at RT, and 61.88±0.03 min. at 10 °C for Ho@C_{82}, respectively. Based on the obtained retention time, the adsorption/desorption enthalpy of Tb@C_{82} and Ho@C_{82} to a pyrenyl stationary phase using toluene as an effluent was evaluated from van't Hoff plot and was found to be 8.07 kJ/mol and 8.08 kJ/mol, respectively. The adsorption/desorption enthalpy of Tb@C_{82} estimated in the previous experiment was about 8.7 kJ/mol, but it is thought that there was a large error in the corrected value because data could not be acquired at the same time as Ho@C_{82}, which has a short half-life.

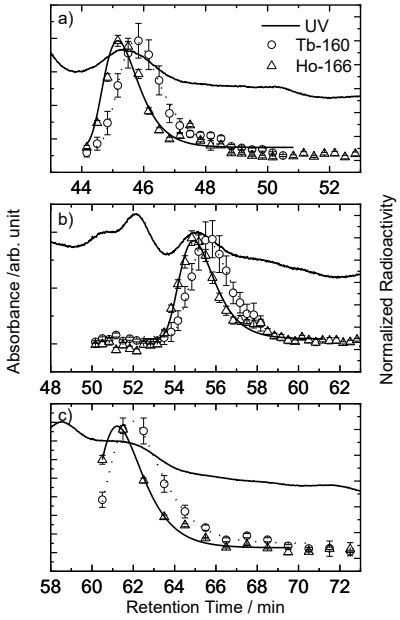

Fig. HPLC chromatograms of Tb and Ho fullerenes developed at a) 40 oC, b) RT, and c) 10 oC.

REFERENCES:

[1] H. Shinohara, Rep. Prog. Phys. 63 (2000) 843-892.
[2] K. Akiyama et al., KURNS Prog. Rep. 2022 CO4-1.

CO4-16

Change in momentum distribution of electrons in Mg_2Sn induced by Sb doping

T. Sumi[1], M. Kitaura[2], A. Kinomura[3], Zhicheng Huang[4], Kei Hayashi[4], Yuzuru Miyazaki[4]

[1]*Graduate School of Science and Engineering, Yamagata University*
[2]*Faculty of Science, Yamagata University*
[3]*Institute for Integrated Radiation Nuclear Science, Kyoto University*
[4]*Graduate School of Engineering, Tohoku University*

INTRODUCTION: Mg_2Sn is known as a Kankyo semiconductor which constituents naturally abundant and environmentally friendly elements. This material has been studied as a candidate for a thermoelectric substance in middle-temperature range (600-900 K) [1]. Sb doping induced the increase in n-type conductivity and thermal conductivity. These parameters have a trade-off relationship in the formula of the figure of merit *ZT*, so it is difficult to improve the ZT through Sb doping. Another phenomenon due to Sb doping attracts attention as an effective method for improving the ZT, because the Sb doping induces the formation of a nano-size region with slightly different lattice constant from Mg_2Sn, which causes the decrease in thermal conductivity due to phonon scattering [2]. The origin of such nano-size region remains unclear at present. In the present study, we have performed positron coincidence Doppler broadening of undoped and 1% Sb doped Mg_2Sn, which provide us the information on the local structure of vacancy-type defects introduced by Sb doping.

EXPERIMENTS: The polycrystals of undoped and 1% Sb doped Mg_2Sn were used as samples. The CDB experiment was performed at the low-energy positron beamline in KUR. The incident energy of the positron beam was 25 keV. The measurements of CDB curves were carried out until the total count of gamma-rays, generating by pair annihilation of positrons with electrons, reaches to 2×10^5 counts. The CDB curves of Mg, Sb, and Sn plates were also measured to use references. The ratio curves of undoped and 1% Sb doped Mg_2Sn, Sb, and Sn relative to Mg were obtained to compare the similarity in CDB curves between these samples, which enables the site identification of vacancy-type defects in undoped and 1% Sb doped Mg_2Sn.

RESULTS: The ratio curves of undoped and 1% Sb doped Mg_2Sn, Sb, and Sn relative to Mg are shown in Fig. 1. The ratio curves of undoped and 1% Sb doped Mg_2Sn are almost the same in the momentum below 7×10^{-3} *mc*. In higher momentum region, the ratio curves are different: The ratio curve of the undoped Mg_2Sn is larger than that of the 1% Sb doped Mg_2Sn. In this region, since the contribution of Sn core electrons is larger than that of Sb core electrons, Sb atoms distribute in high concentration around vacancy-type defects in 1% Sb doped Mg_2Sn. From positron annihilation lifetime spectroscopy experiments, it was turned out that Mg vacancies are introduced by Sb doping. Based on the results obtained, it is likely that the defect complexes of Sb atoms and Mg vacancies are formed in the nano-size region.

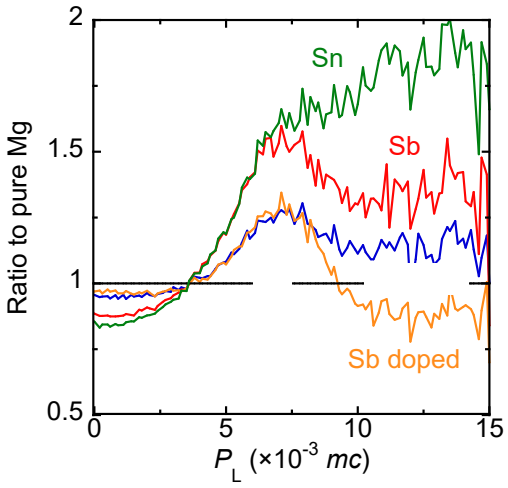

Fig.1 Ratio curves of undoped and 1% Sb doped Mg_2Sn relative to that of Mg. The ratio curves of Sb and Sb were also shown for references.

REFERENCES:

[1] D. Shiojiri *et al.*, Energies, **15** (2022) 4859.
[2] W. Saito et al., ACS Appl. Mater. Interface **12** (2020). 57888.

CO4-17

Strength properties and microstructure/orientation dependence of irradiation defect formation behavior in tungsten materials

K. Tokunaga[1] and Q. Xu[2]

[1] *Research Institute for Applied Mechanics, Kyushu University*
[2] *Institute for Integrated Radiation and Nuclear Science, Kyoto University*

INTRODUCTION: Tungsten (W), which exhibits excellent thermal properties and low sputtering yield, is a promising candidate for plasma-facing materials in the divertor in fusion reactors. The microstructure and the distribution of pre-existing defects in W strongly depend on the manufacturing process, leading to significant variations in structure-sensitive properties such as mechanical strength and irradiation-induced defect formation behavior. In this study, specimens have been prepared from pure rolled W (ITER divertor-grade, stress-relieved) by cutting along different orientations to vary the microstructure and the alignment of pre-existing defects. These specimens have been subjected to electron irradiation experiments to investigate defect formation behavior.

EXPERIMENTS: Specimens will be extracted from rolled pure tungsten (ITER divertor grade, stress-relieved) along different crystallographic orientations. These specimens will be irradiated with an electron beam using the LINAC at the Kyoto University Institute for Integrated Radiation and Nuclear Science. Before and after irradiation, positron annihilation spectroscopy will be employed to identify pre-existing and irradiation-induced defects. Electron backscatter diffraction (EBSD) has been used to analyze the microstructure and crystallographic orientations.

RESULTS: Figure 1 shows the planes with respect to the rolling direction. Figure 2 presents the IPF map (ND) obtained by EBSD. On the TD plane, which is perpendicular to the rolling plane and parallel to the rolling direction, it can be observed that the grains are elongated along the rolling direction. Figure 3 shows the positron lifetime measurement results for each plane. The results differ depending on the plane. In particular, for the TD plane, the lifetime of τ_2 is longer, while its intensity (I_2) is lower compared to those of the other planes. The positron lifetimes for defect-free W and a monovacancy are 110 ps and 180 ps, respectively. The τ_1 values for the ND and RD planes are close to that of defect-free W. These results indicate that, on the TD plane, vacancies exist in the form of vacancy clusters, although their concentration is low. It is considered that vacancy clusters are more likely to grow during the elongation process of grains on the TD plane. Thus, it was found that rolled tungsten exhibits differences even in its microscopic structure as measured by positron lifetime spectroscopy. In future work, electron irradiation will be performed on these specimens to clarify the defect formation processes.

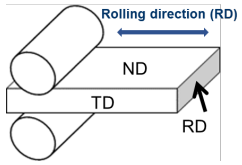

Fig. 1 Orientation of rolling

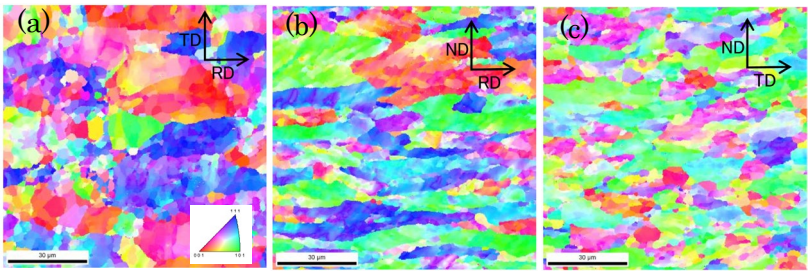

Fig. 2. IPF-map(ND) (a):ND, (b):TD, (C)RD

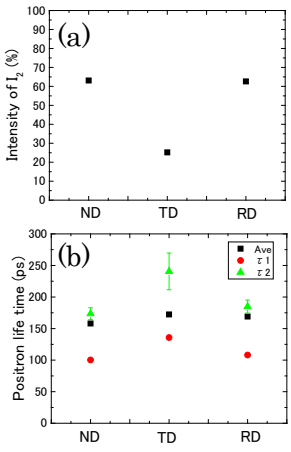

Fig. 3. Intensity of I_2(a) and positron life time(b).

CO4-18

Research on freezing of materials under high pressure by Bessel-beam driven micro-explosions in transparent materials

H. Nakamura[1], T. Iwamoto[1], R. Utsunomiya[1], Y. Nakanishi[1], N. Yamagata[1], T. Pikuz[1], T. Okuchi[2], Y. Umeda[2], L. Rapp[3], A. Rode[3], T. Shobu[4], A. Tominaga[4], Y. Seto[5], R. Kodama[1], N. Ozaki[1]

[1] *Graduate School of Engineering, The University of Osaka*
[2] *Institute for Integrated Radiation and Nuclear Science, Kyoto University*
[3] *Australian National University*
[4] *Japan Atomic Energy Agency*
[5] *Graduate School & School of Science, Osaka Metropolitan University*

INTRODUCTION: It is possible to create extreme pressure and temperature conditions in the tabletop laboratory experiments with 100-fs ultra-short laser pulses focused inside a transparent material, with intensity in the focal spot significantly above the threshold for optical breakdown [1]. Tight focusing of a laser pulse with a few micro-Joule energy deep inside a crystal can deposit an energy density up to several MJ/cm^3 in a sub-micron volume. Pressure created by the plasma expansion is high enough to generate new material phases, which is referred to as micro-explosion [2 ,3]. Here we report an experiment relative to a micro-explosion with a layered target made of Al_2O_3 and highly ordered pyrolytic graphite (HOPG). Hence, we demonstrated X-ray diffraction (XRD) analysis of the material under high pressure and high temperature phase.

EXPERIMENTS:

(1) Micro-explosions experiment with femtosecond laser

The beam of a 250 fs amplified Ti:Sapphire laser with a central wavelength of 800 nm was focused on the surface of HOPG. The energy and spot size were 200 nJ and 1.2 μm, respectively. After laser processing, the structures of void on the surface of HOPG were observed with Scanning Electron Microscope (SEM).

(2) XRD analysis with by Rigaku Ultima IV at KURNS

XRD analysis was demonstrated with the material with void formed inside by micro-explosions to observe high pressure phase of (Diamond and/or Lonsdaleite). X-ray energy was 8.04 keV (Cu-Kα).

RESULTS:

Results of observation of void structure with SEM shows the length and diameter were 10 μm and 350 nm, respectively. The volume of the void is ~2 femtolitres.

Figure 1 shows the results of XRD. Signal of 2θ diffraction with angles of 44.5 and 64.45 degrees. These observations indicate the signals derived from carbon high pressure phase. Further analyses are underway to better understand the data.

REFERENCES:

[1] S. Juodkazis, et al., Phys. Rev. Lett. 96, 166101 (2006).
[2] A. Vailionis, et al., Nat. Commun. 2, 445(2011).
[3] L. Rapp, et al., Sci. Rep. 6, 34286 (2016).

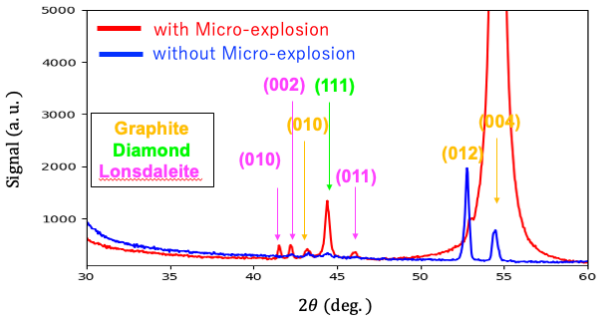

Fig. 1. XRD result

CO4-19

Elucidation of the Dynamics of Rigid Helical Polymers in Hydrocarbon Solvents by Small-Angle X-Ray Scattering and Molecular Dynamics Simulations

Y. Nagata[1], M. Sugiyama[2], R. Inoue[2], N. Sato[2], and K. Morishima[2]

[1] *Research Center for Macromolecules and Biomaterials, National Institute for Materials Science*
[2] *Institute for Integrated Radiation and Nuclear Science, Kyoto University*

INTRODUCTION: Poly(quinoxaline-2,3-diyl)s, which are denoted as PQXs, constitute a class of rigid helical polymers that exhibit solvent-dependent switching of helical chirality. Previous studies have shown that PQXs bearing chiral alkoxymethyl side chains adopt different helical conformations in response to changes in the solvent environment. In particular, a 100-mer PQX bearing (*R*)-2-octyloxymethyl side chains adopts a right-handed helical structure in tetrahydrofuran and an *M*-helical structure in a mixed solvent composed of 1,1,2-trichloroethane and tetrahydrofuran.[1] Small-angle neutron scattering (SANS)[2] and quasielastic neutron scattering measurements (QENS),[3] combined with molecular dynamics (MD) simulations, have indicated that the spatial arrangement and mobility of the side chains are closely related to the inversion of helical handedness.

Solvent-induced helix inversion has also been observed for PQXs in simple saturated hydrocarbon solvents. A PQX bearing (*S*)-3-octyloxymethyl side chains exhibits an *M*-helical structure in *n*-octane and a *P*-helical structure in cyclooctane. This behavior is remarkable because the inversion is induced by a subtle change between alkane solvents. However, the molecular mechanism by which hydrocarbon solvents control the helical structure remains insufficiently clarified. In the present study, we investigated the structure and dynamics of a 100-mer PQX bearing (*S*)-3-octyloxymethyl side chains (**3oct**) in hydrocarbon solvents by combining SANS experiments with molecular modeling.

EXPERIMENTS AND RESULTS: Initially, the structures of the repeating monomeric units, which comprise two conformational isomers designated as the δ-monomer and λ-monomer, were optimized using the Forcite optimizer in BIOVIA Materials Studio 2024 with the COMPASS III force field at the ultra-fine level. Based on these optimized monomers, right-handed and left-handed 100-mer helical structures, namely *P*-δ-**3oct**, *M*-δ-**3oct**, *P*-λ-**3oct,** and *M*-λ-**3oct**, were constructed and further optimized. For these optimized structural models, small-angle neutron scattering spectra in *n*-octane-d_{18} were simulated using software developed by Prof. Sugiyama. The simulated scattering profiles were then compared with the experimental SANS data (Fig. 1). The present structural models did not provide satisfactory agreement with the measured profiles. This discrepancy indicates that further refinement of the molecular structures is required in order to reproduce the experimentally observed conformations in solution. Future work will involve a comprehensive conformational search and molecular dynamics simulations to identify structural models that can more accurately describe the scattering behavior of the (*S*)-3-octyloxymethyl-substituted PQX in hydrocarbon solvents.

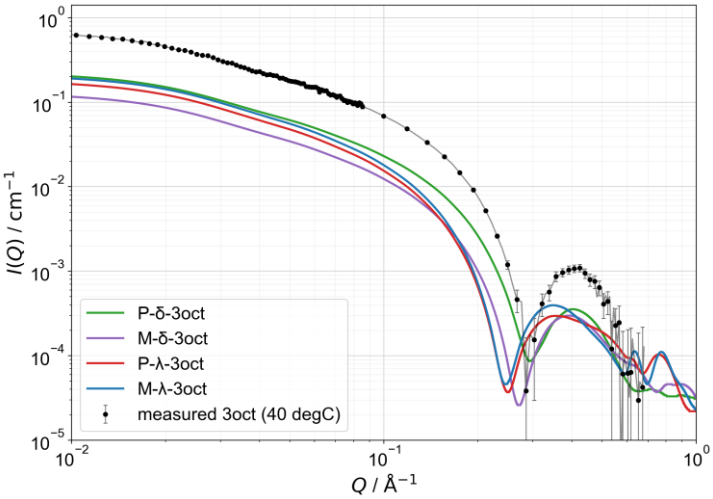

Fig. 1. Log-log SANS profiles of measured **3oct** at 40 °C and four simulated conformations in *n*-octane-*d*18.

REFERENCES:

(1) Nagata, Y.; Yamada, T.; Adachi, T.; Akai, Y.; Yamamoto, T.; Suginome, M. *J. Am. Chem. Soc.* **2013**, *135*, 10104–10113.
(2) Nagata, Y.; Nishikawa, T.; Suginome, M.; Sato, S.; Sugiyama, M.; Porcar, L.; Martel, A.; Inoue, R.; Sato, N. *J. Am. Chem. Soc.* **2018**, *140*, 2722–2726.
(3) Inoue, R.; Nagata, Y.; Tominaga, T.; Sato, S.; Kawakita, Y.; Yamawaki, T.; Morishima, K.; Suginome, M.; Sugiyama, M. *J. Chem. Phys.* **2024**, *161*, 054905.
(4) Nagata, Y.; Nishikawa, T.; Suginome, M. *J. Am. Chem. Soc.* **2014**, *136*, 15901–15904.

CO4-20

Positron annihilation study of electron irradiation-induced vacancy defects in CoCrFeNi medium-entropy alloy

H. Araki[1], M. Mizuno[1] and A. Kinomura[2]
[1] *Graduate School of Engineering, The University of Osaka*
[2] *Institute for Integrated Radiation and Nuclear Science, Kyoto University*

INTRODUCTION: Tsai *et al*. [1] reported sluggish diffusion in the CoCrFeMnNi high-entropy alloy (HEA), although its mechanism remains unclear. Because the HEA and its subsystems form substitutional solid solutions, the diffusion is expected to occur mainly via a vacancy mechanism, making vacancy formation and migration energies essential to understanding sluggish diffusion. In this study, we estimate the vacancy migration energy in the CoCrFeNi medium-entropy alloy by analyzing vacancy migration and annihilation during post-irradiation annealing.
EXPERIMENTS: An arc-melted ingot of the CoCrFeNi alloy was homogenized at 1373 K for 24 h under an argon atmosphere and subsequently cut into plates with dimensions of 10 mm × 10 mm × 0.5 mm. The plates were mechanically polished and sealed in silica tubes. Solution heat treatment was then performed at 1373 K for 1 h, followed by water quenching. X-ray diffraction analysis confirmed that all samples consisted of a single face-centered cubic (fcc) phase. The samples were irradiated in water with 8 MeV electrons to a fluence of approximately 1×10^{22} e^{-} m^{-2} at temperatures below 358 K, using the electron linear accelerator at the Institute for Integrated Radiation and Nuclear Science, Kyoto University. Isochronal annealing was subsequently conducted between 373 and 673 K in 25 K increments, with each annealing step lasting 1 h. Positron lifetime measurements were carried out at 297–299 K using a fast–fast timing coincidence system with a time resolution (FWHM) of 180–183 ps.
RESULTS: Before electron irradiation, the positron lifetime spectrum of the solution-treated alloy was characterized by a single lifetime component of 108 ps, indicating that positron annihilation occurs predominantly in the defect-free bulk. After irradiation, the mean positron lifetime increased to 133 ps. Analysis of the irradiated sample shows that a substantial fraction of positrons are trapped and annihilate in monovacancies introduced by electron irradiation, as evidenced by the trapped-positron lifetime component of 180 ps. Assuming a specific trapping rate for monovacancies of μ_v=10^{15} s^{-1}, the vacancy concentration in the irradiated alloy is estimated to be on the order of several atomic parts per million. The evolution of vacancy concentration during isochronal annealing was evaluated using two- or three-component analyses of the positron lifetime spectra. In the temperature range where both dislocations and monovacancies are expected to coexist, the spectra were analyzed by assuming a positron lifetime of 150 ps for dislocations. The vacancy concentration decreases with increasing annealing temperature because vacancies introduced by irradiation gradually disappear as they become mobile during isochronal annealing. The decrease in vacancy concentration was further examined using the isothermal annealing model proposed by Dryzek *et al*. [2]. When a single, temperature-independent vacancy migration energy is assumed, noticeable discrepancies arise between the theoretical fitting and the experimental data. Positron lifetime measurements at higher temperatures reveal the presence of dislocation loop–related components, suggesting that vacancy migration is strongly affected by dislocations. To account for this effect, two vacancy migration energies, $H_m{}^L$ and $H_m{}^H$, were introduced and optimized to reproduce the experimental behavior. The value obtained for $H_m{}^L$ in the low-temperature region is 0.92 eV, which is nearly identical to the reported migration energy of 0.93 eV for vacancies in CoCrFeMnNi [3].
REFERENCES:
[1] K. Y. Tsai, M. H. Tsai and J. W. Yeh, Acta Mater., 61 (2013) 4887.
[2] J. Dryzek, C. Wesseling, E. Dryzek and B. Cleff, Mater. Lett., 21 (1994) 209.
[3] K. Sugita, R. Ogawa, M. Mizuno, H. Araki and A. Yabuuchi, Scripta Mater., 208 (2022) 114339.

CO4-21

Influence of Hydrogen Isotopes on Growth of Vacancy Clusters in Tungsten-Based Materials

Y. Hatano[1], E. Taguchi[1], A. Matsumoto[1], Q. Chen[1], T. Takahashi[2], N. Abe[2] and A. Kinomura[2]

[1] *Graduate School of Engineering, Tohoku University*
[2] *Institute for Integrated Radiation and Nuclear Science, Kyoto University*

INTRODUCTION: Tungsten (W), a plasma-facing material in fusion reactors, is exposed to hydrogen isotopes (deuterium and tritium) and fusion reaction products such as helium and 14 MeV neutrons. Vacancies and vacancy clusters created by neutron irradiation act as strong traps for hydrogen isotopes, leading to increased tritium retention in W [1]. Therefore, understanding vacancy formation and clustering is essential for accurate evaluation of tritium inventory in the vacuum vessel of fusion reactors. Since displacement damage develops under simultaneous exposure to hydrogen isotope plasma, hydrogen isotopes may influence the evolution of vacancy clusters. The objective of this study is to clarify the effects of hydrogen isotopes on vacancy and vacancy-cluster evolution, with the aim of developing a kinetic model for clustering and annihilation processes. To achieve this, W samples containing vacancy clusters were prepared by electron-beam irradiation, followed by annealing with and without hydrogen exposure. Changes in vacancy-cluster size distributions were investigated using positron annihilation spectroscopy (PAS).

EXPERIMENTS: Disk-shaped W samples were irradiated with 8 MeV electrons using KURNS-LINAC to 10^{-3} displacement per atom (dpa). A portion of irradiated samples was exposed to hydrogen (H) atoms at 200 ℃ and then heated under H_2 gas atmosphere (0.1 MPa) at 400 and 500 ℃ for 20–40 h. The remaining samples, without H exposure, were annealed under otherwise identical conditions. Positron lifetime was measured using a ^{22}Na source [1].

RESULTS AND DISCUSSION: The positron lifetime spectra were well fitted by the sum of two exponential decay components: a short lifetime of approximately 150 ps and a long lifetime of approximately 350 ps. The former corresponds to the annihilation in the defect-free W lattice, whereas the latter is attributed to annihilation at vacancy clusters consisting of roughly 10 vacancies [2]. Annealing at 400 ℃ resulted in no significant change in positron lifetime for either sample. After annealing at 500 ℃ for 40 h, the H-free sample exhibited a clear increase in the long-lifetime component to approximately 400 ps, which is attributed to Ostwald ripening of vacancy clusters. However, no significant change was observed in the H-exposed sample. This difference indicates that the presence of H suppressed the growth of vacancy clusters. It is plausible that H atoms inhibited decomposition of small vacancy clusters and subsequent growth into larger clusters.

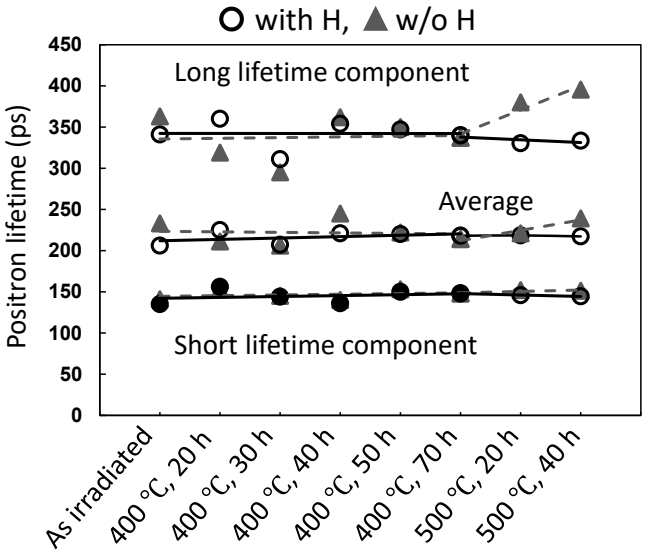

Fig. 1 Change in positron lifetime in electron-irradiated W after heating with and w/o H.

REFERENCES:

[1] T. Toyama et al., J. Nucl. Mater., 499 (2018) 464.
[2] T. Troev et al., Nucl, Instr. Meth. B, 267(2009)535.

CO4-22

Chemical information contained in X-rays emitted during radioactive decay and its applications

H. Kikunaga[1], K. Takamiya [2] and M. Inagaki[2]

[1] *Research Center for Accelerator and Radioisotope Science*
[2] *Kyoto University Institute for Integrated Radiation and Nuclear Science*

INTRODUCTION: As radioactive isotopes (RI) emit radiation from individual atomic nuclei, they offer extremely high detection sensitivity, making it possible to detect even minute quantities. Furthermore, activation analysis, which utilises neutrons from nuclear reactors, is widely recognised as a non-destructive analytical method capable of achieving sensitivity at the ppb level for many elements and quantifying multiple elements simultaneously. However, both RI tracer methods and activation analysis are quantitative techniques and cannot identify the chemical state.
We investigate the chemical information contained in the X-rays emitted during radioactive decay. When a RI decays, beta and gamma rays are emitted alongside the nuclear decay, and X-rays are emitted during electronic transitions. Here, we focus on X-rays associated with outer-shell electrons, which are influenced by the chemical state. Whilst we have previously acquired fundamental data using tracers produced by an accelerator, the aim of this study is to obtain data on samples that have been neutron-activated.

EXPERIMENTS: Samples consisting of powders of metals and compounds such as copper, manganese, iron and chromium were irradiated at KUR using Tc-Pn and Pn2. The post-irradiation samples were spread as thinly as possible between adhesive tapes and sealed to form measurement sources. Measurements were performed in the X-ray and γ-ray regions using a silicon drift detector and a high-purity germanium semiconductor detector. The output from these detectors was sent to a digital MCA, and measurements were carried out in list mode.

RESULTS: Although the results are currently being analysed, the spectra obtained show not only X-rays associated with radioactive decay but also X-ray signals generated when the emitted radiation excites the constituent materials of the radiation source and other components. It is necessary to carefully analyse whether the variations in the spectra observed for different radiation sources are due to changes in the chemical state or to changes in the surrounding materials.

ACKNOWLEDGMENT:
This work was supported by JSPS KAKENHI Grant Number JP 23K17684

CO4-23

Magnetic Measurements of Irons in new Si-based Ferrite-like Functional Materials using In-flight Melting Materials Method by Mössbauer Spectroscopy

K. Okada[1] and Y. Kobayashi[2]

[1]*SPring-8,* [2]*Graduate School of Engineering, Kyoto University*

INTRODUCTION: Glass is used in many applications in our every-day lives and has exciting new applications related to the energy. Soda-lime glass is made of mainly silica (SiO_2) and additive many other materials, such as magnesium, sodium, calcium, aluminum, iron, sulfur, and so on. Our reference glass composition, in percent by weight (wt%), was 72.25 SiO_2, 1.75 Al_2O_3, 4.00 MgO, 8.00 CaO, 14.00 Na_2O as basic components, and 0.015-5 iron in terms of Fe_2O_3 as coloring components. Iron contaminants of less than 0.0005-0.01 wt% from raw materials, and iron injection up to 1.5-5 wt%. We added compatible $CaCO_3$ and Na_2CO_3 as CaO and Na_2O, respectively. The iron oxides in a glass composition are thought to be present in forms of Fe^{3+} and Fe^{2+}. The control parameters for irons are two: (1) the total iron mass weight percent in terms of Fe_2O_3, and (2) the ratio of $Fe^{2+}$to total iron ions (Fe^{2+}/Σ_nFe). The Fe^{3+} component adds a light yellow tint to the glass and absorption in the ultraviolet and visible band, while the Fe^{2+} component adds a blue tint to the glass and absorption in the near-infrared band (1 μm). The transmission from ultraviolet to infrared in glass cannot be explained by simple Fe^{2+} and Fe^{3+} structures. Then, to reveal the exact local structures of irons (Fe^{2+} and Fe^{3+}) is necessary. Many scientists proposed many new theories and local structures [1-2], but they did not resolve it completely.

We have prepared reference glass samples with using the Mössbauer isotope ^{57}Fe (natural abundance is about 2.119 %) for measurements. The chemical composition of iron oxide in the ^{57}Fe enrichment glass was from 0.015 to 5 wt%, and the Fe^{2+}/Σ_nFe was from 0 to 0.6. We have investigated these samples by nuclear resonant inelastic scattering and XAFS methods at synchrotron radiation to reveal the local atomic structure around and neighboring iron in sub-nanometer region [3].

We also have prepared new amorphous-Si-based functional glass and semi-melted crystal-like materials with iron, whose chemical composition was the same with the reference glass, for new scientific purposes[4-8], by in-flight melting material method[4-5]. We have also succeeded to make Ferrite-like materials by fast melting and fast cooling cycles[6-7]. We have thought that the high temperature in melting process and their chemical components were similar to those of fly-ash, although the assumed iron-oxides in the Yonden fly-ash was ~1 to ~10(-30) wt%.

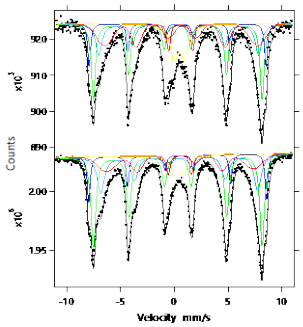

Fig. 1. Mössbauer spectra of Yonden fly-ash collecting with/ without (lower/upper panel) the magnetic stirrer bar in slurry.

EXPERIMENTS: We observed two-type black-colored components in Yonden fly-ash gathering with and without the magnetic stirrer bar in a water slurry, because it is difficult to gather black-colored ones directly from the dried fly-ash. The measurements were performed using conventional Mössbauer spectrometer at 273K. The specimens for Mössbauer measurements were tuned to 10 mm-phi pellet.

RESULTS: There was no typical difference between the two-type samples collecting with and without magnet as shown in Fig. 1. Most black-colored components in Yonden fly-ash were thought to be Hematite, Maghemite + Magnetite. Iron oxides in the Yonden fly-ash are integrated with Si (and O), and they are considered to exist rarely as separate particles, which are easy to collect with magnetic tools.

REFERENCES:

[1] C. Ruessel, *et al.*, *Phys. Chem. Glasses*,**47** (2006)563. [2] F. Farges, *et al.*, *Physica Scripta*, **T115**(2005)957. [3] K. Okada, *et al.*, X-ray Spectrometry, **47**(2018)359-371 [4] K. Okada, *et al.*, J. Ceram. Soc. Japan, **130[06]**(2022) S1-S6. [5] K. Okada, *et al.*, J. Ceram. Soc. Japan, **128**(2020)981-990 [6] K. Okada, *et al.*, https://pub.confit.atlas.jp/ja/event/jsap2024s/presentation/25a-32A-10 [7] K. Okada, *et al.*, https://confit.atlas.jp/guide/event/jsap2023s/subject/15p-D505-13/detail [8] https://nrid.nii.ac.jp/ja/nrid/1000070399616/
https://researchmap.jp/Okada-Kyoko_Physics physics.materials.science@gmail.com

CO4-24

Development of New-type Diamond Detectors for Neutron

K. Okada[1], K. Takamiya[2], Y. Kobayashi[2] and Y. Sakurai1[2]
[1] *SPring-8,* [2] *Institute for Integrated Radiation and Nuclear Science, Kyoto University*

INTRODUCTION: The diamond is 5.47 eV wide-gap semiconductor with high radiation resistance and thermal conductivity. Diamond detector has energy resolution. Then we developed new-type single/multiple crystal diamond detectors for gamma-ray/x-ray or alpha particles/neutron detection. We proposed these detectors for astrophysics, medical applications and nuclear reactor operations. We planned to arrange these diamond devices with special short wavelength and ultra short pulsed (femtosecond to picosecond range) laser machines. [1-4] First, we developed normal-type single crystal diamond detectors for x/gamma rays and alpha-particles. We first used the much high quality CVD diamond plate, which was homo-epitaxial grown using a microwave plasma chemical vapor deposition (MPCVD). We also used the HPHT diamond plate for comparison, Then we developed simple transmission-type detectors with double-sided illumination capability as sown in Fig. 1. We succeeded to develop new-type single crystal double-sided illumination diamond detectors for only alpha particles detection with normal diamond plate. Then, we used this diamond detector for neutron detection by converting to alpha-particles with Boron (^{10}B) material on the thin electrode of the detector. We also especially planned the large area-size multiple/polycrystalline diamond detectors for single-use, which are required for decommissioning works at Fukushima. Then we proposed new plasma/thermal filament method to make CVD multiple diamond with original electrodes for new-type diamond detectors with simple production. [5-6]

EXPERIMENTS: This time, we used single/multiple diamond crystal by plasma CVD method and HPHT method. The size of the diamond plate was from 2x2 mm to 10x10 mm. We made the same Ti(30nm)/Pt(30nm)/Au(100nm) electrodes on both sides of the diamond plate. At one side, we made guard-ring on one electrode. We coated thin boron (^{10}B) materials (BN powders) on a thin electrode (Ti(30nm)/Pt(30nm)/Au(100nm)) without guard-ring to convert neutron to alpha particles. We used this detector with low noise amplifier (CP-580H etc) as shown Fig.2. We observed thermal neutron in the Heavy Water Neutron Irrdadiatipn Facility of Kyoto University Reactor (KUR).

RESULTS: We succeeded to detect neutron signals continuously as shown in Fig. 2 (see pulse shape in the Oscillo scope window). However, within a few minutes, we also observed cyclic current increasing and decreasing without additional pulsed signals. We did not find causes at all. The base metal plate and substrate materials of our diamond detector were not adequate for neutron experiments. These materials have become radioactive as shown in Fig. 3. The prompt gamma rays emitted from ^{198}Au are particularly noticeable

REFERENCES:

[1]https://pub.confit.atlas.jp/ja/event/jsap2024s/presentation/23p-13M-17,
[2]https://confit.atlas.jp/guide/event/jsap2023s/subject/17a-E502-7/detail）[3] https://nrid.nii.ac.jp/ja/nrid/1000070399616/
[4] https://researchmap.jp/Okada-Kyoko_Physics physics.materials.science@gmail.com
[5] https://nanonet.go.jp/user_report.php?mode=detail&code=10688&key=3wOdtF2aDPcZ7fpa
[6] https://nanonet.go.jp/user_report.php 25SH0002

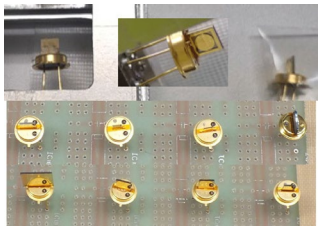

Fig.1 Diamond detectors.

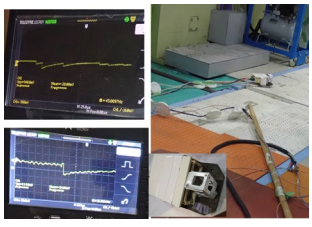

Fig.2. Signals and setup

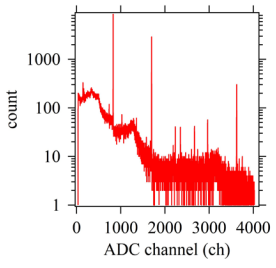

Fig.3. Activation of the case

CO4-25

Effect of zirconium on the tritium release behavior from neutron-irradiated $LiAlO_2$

K. Katayama[1], H. Isogawa[2], R. Ganaha[2], K. Akashi[3], H. Matsuura[3] and Y. Iinuma[4]

[1]*Faculty of Engineering Science, Kyushu University*
[2]*Interdisciplinary Graduate School of Engineering Sciences, Kyushu University*
[2]*Faculty of Engineering, Kyushu University*
[3]*Institute for Integrated Radiation and Nuclear Science, Kyoto University*

INTRODUCTION: Tritium (T) production using a high-temperature gas-cooled reactor (HTGR) has been proposed to arrange initial T inventory for nuclear fusion reactors [1]. By loading Li-rods in place of Burnable-Poison-rods, T can be produced without significant modifications to the original structural design of HTGRs. One concern is the permeation loss of T at high temperature conditions. In the recent design, the Li rods consist of an alumina container installing $LiAlO_2$ and Zr pebbles. Zr pebbles play the role of absorbing tritium released from $LiAlO_2$ and reducing the tritium partial pressure inside the alumina container. To evaluate the tritium confinement performance of the Li rod structure, it is necessary to understand the tritium behavior in an environment where $LiAlO_2$ an Zr coexist. In this study, neutron-irradiated $LiAlO_2$ was heated in the presence of Zr, and the behavior of the released tritium was observed.

EXPERIMENTS: The powdered $LiAlO_2$ was packed into a quartz tube in vacuum and irradiated neutrons with a flux of 2.75×10^{13} n/(cm^2·s) for 3 minutes at KUR. After neutron irradiation, the samples were transported to Kyushu University for tritium release experiments. The schematic diagram of the experimental apparatus is shown in Fig.1. The neutron irradiated $LiAlO_2$ with broken quartz tube was packed with Zr pebbles in a quartz reaction tube. The $LiAlO_2$ with Zr pebbles was heated by an electric furnace to 900 °C in Ar gas flow. The tritiated water vapor (HTO) and gaseous tritium (HT) were separately collected in water bubblers. The bubblers was replaced every 5 minutes and tritium concentration was measured by a liquid scintillation counter.

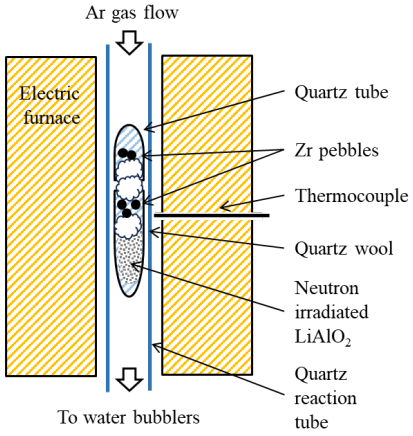

Fig.1. Experimental apparatus.

RESULTS: The release rate of HT and HTO was shown in Fig.1. HTO was released with the onset of heating, and the release rate peaked around 250 °C and then gradually decreased. HT was released from around 500 °C and the release rate peaked at around 750 °C and then sharply decreased. In the absence of Zr pebbles, the majority of tritium released from $LiAlO_2$ was observed to be HTO in previous works. The detection of HT suggests that the HTO released from $LiAlO_2$ was reduced to HT through interaction with Zr. The rapid drop in HT release observed above 750 °C is considered to be caused by the accelerated HT absorption into Zr.

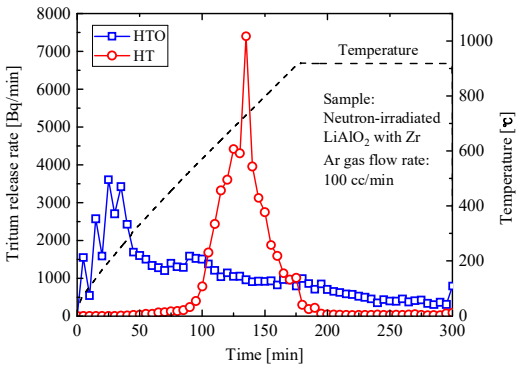

Fig.2. Tritium release from neutron irradiated $LiAlO_2$ in the presence of Zr pebbles.

REFERENCES:

[1] H. Matsuura, et al., Nucl. Eng. Des. **243** (2012) 95–101.

CO4-26

Neutron Irradiation Tests for ITER Diagnostic Systems in JADA

T. Yokozuka[1], T. Kikuchi[1], M. Fukuda[1], K. Nojiri[1], T. Ushiki[1], E. Yatsuka[1], S. Kitazawa[1], R. Imazawa[1], H. Yoshino[2], and K. Takamiya[2]

[1]*Department of ITER Project, Naka Institute for Fusion Science and Technology, National Institutes for Quantum Science and Technology*
[2]*Institute for Integrated Radiation and Nuclear Science. Kyoto University*

INTRODUCTION: ITER is the world's largest fusion experiment reactor and is under construction in southern France [1]. Components of diagnostic systems installed in the ITER tokamak are exposed to high neutron radiation. Therefore, it is important to investigate the effect of neutron irradiation on these components. JADA (ITER project Japan Domestic Agency) have been conducted neutron irradiation tests on components of ITER diagnostic systems in KUR from 2018. In fiscal 2025, neutron irradiation tests were conducted on optical elements used in DIM (Divertor Impurity Monitor) [2]. The effects of neutron irradiation on spectral transmittance and reflectance were measured for optical elements used in a spectrometer placed on a PCSS (Port cell Support Structure) and for optical fibers placed on the PCSS, and their applicability was evaluated. The spectrometers, which use the optical elements, are installed in PCSS at three ports: UP01, EP01, and LP02. The expected fluence was calculated using the ITER radiation map, and then the maximum fluence is 5 x 10^{13} n/cm² at EP01. This evaluation focused on verifying whether the optical elements could withstand this value. The irradiated specimens are one substrate, one dichroic mirror, one dielectric multilayer mirror, and four bandpass filters as optical elements used in the spectrometer, as well as two types of optical fiber strands.

EXPERIMENTS: The neutron irradiation experiment was conducted using Slant Exposure at KUR. The maximum neutron flux during 1 MW operation was 1 x 10^{12} n/cm^2/s. The substrate used was Ohara's SK-1300, made of SiO_2, with dimensions of Φ25.4 mm x 2 mm. The filters and mirrors were prepared by depositing thin films of a combination of HfO_2, Ta_2O_5, Al_2O_3, MgF_2, and ZrO_2.
The optical fiber specimens consist of SiO_2 core, F-doped SiO_2 cladding and polyimide jacket. One type of specimens has an additional carbon layer between cladding and jacket.

RESULTS: The optical transmittance of the substrate in the 200-800 nm range was approximately 90%, and no significant changes were observed before and after irradiation at 5 x 10^{13} n/cm². Figure 1 shows an example of the transmittance spectra of the 372 nm bandpass filter specimen neutron irradiated with neutron. For irradiation up to 5 x 10^{13} n/cm², neither a significant decrease in transmittance nor a peak shift is observed. Figure 2 shows an example of the change in transmission of optical fiber by neutron irradiation, as ratio of value before irradiation. No significant decrease in transmittance is observed for irradiation up to 5 x 10^{13} n/cm².

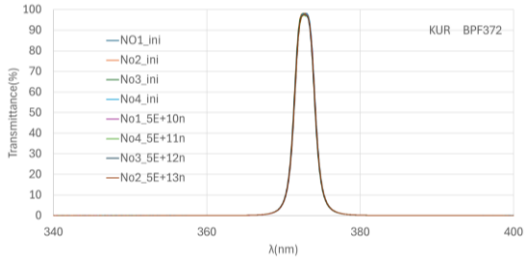

Fig. 1 Transmission spectrum of 372nm bandpass filter specimen irradiated with neutrons

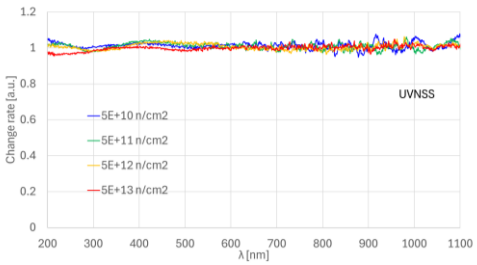

Fig. 2 Transmission of optical fiber by neutron irradiation

REFERENCES:

[1] https://www.iter.org
[2] S. Kitazawa, *et al.*, Plasma and Fusion Research 14(2019) 3405089.

CO4-27

Lithium Vacancy Concentrations Measurements in Positive Electrodes of Charged and Discharged-Lithium Ion Batteries Using Positron Annihilation Spectroscopy

B. Tsuchiya[1], R. Terasawa[1], K. Kataoka[1], A. Kinomura[2] and T. Sasaki[3]

[1] *Division of Materials Science and Engineering, Graduate School of Science and Technology, Meijo University, Nagoya 468-8502, Japan*

[2] *Institute for Integrated Radiation and Nuclear Science, Kyoto University (KURNS), Kumatori-cho, Osaka, 590-0494, Japan*

[3] *Institute for Materials Research, Tohoku University, 2-1-1, Katahira, Aoba-ku, Sendai 980-8577, Japan*

INTRODUCTION: An oxide-based solid-state rechargeable lithium ion (Li^+) battery is one of the most remarkable next generation devices. To realize the product, it is essential that we have information on the Li^+ ion transfer resistance at electrode/solid electrolyte interfaces and grain boundaries in the solid-state Li^+ ion batteries. In particulr, the Li deficient region formed around the interface during the charging and discharging, which is indicative of space charge layer, locally provides less Li^+ ion conduction and then leads to the interfacial Li^+ ion transfer resistance, since the Li^+ ionic conductivity in the solid electrolyte significantly depends on the number of Li^+ ion mobile carriers. Thus, the Li distribution around interface in static or operated solid-state Li^+ ion batteries should be clarified well [1].

EXPERIMENTS: Some Li^+ ion rechargeable batteries consisting of the $LiCoO_2$ positive electrode and the Li negative electrode with a dimension of 30 mm × 35 mm × 105 μm, including the $LiPF_6$ electrolyte, were built up by JFE Techno-Research Corporation. Six types of Li_xCoO_2 samples with different x values were prepared for as-received (no bias, x = 0.99), break-in by SoC 0% (0% charge, x = 0.99), charged by SoC 50% (50% charge, x = 0.73) and SoC 100% (100% charge, x = 0.49), and charged by SoC 100% and subsequently discharged by SoC 50% (50% discharge, x = 0.74) and SoC 0% (100% discharge, x = 0.99). Next, positron annihilation spectroscopy (PAS), which was useful technique that enables investigating the behavior of voids in the materials, was employed using energy-variable monoenergetic positron beams (slow positron beams) of KUR-ISOL (B1 port) from the fission reactor with 5 MW, installed at Institute for Integrated Radiation and Nuclear Science, Kyoto University.

RESULTS: Figure 1 shows Li vacancy concentrations in no bias, charged (SoC 0, 50, and 100%), and charged-discharged (SoC 50 and 0%) Li_xCoO_2 ($0.49 \leq x \leq 0.99$) as a function of the depth from the topmost surface. The depth distributions of the Li vacancy increased and decreased, respectively, at each depth by charging and discharging. They are in good agreement with the amounts of Li^+ ion transfer and Li concentrations, respectively, obtained from electrochemical measurements and ERD technique. In particular, it was found that the amounts of the Li vacancies increased with the gradient in the near surface of Li_xCoO_2.

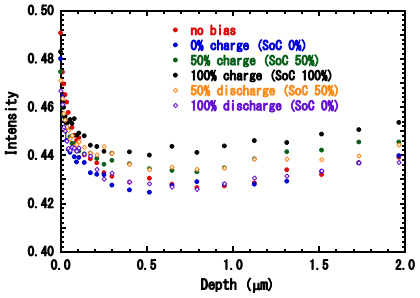

Fig. 1. Li vacancy concentrations in Li_xCoO_2 samples (x = 0.49 – 0.99), charged and discharged with 40 mA for each time.

REFERENCES:

[1] M.G.S.R. Thomas, P.G. Bruce, J.B. Goodenough., Solid State Ion., **17** (1985) 13-19.

CO4-28

Acoustic velocities of silicate glass under ultra-high pressure

P. Saha[1], M. Murakami[1], P. A. Sossi, S. Kitao[2], M. Seto[2], T. Mitsui[3], P. Lefebvre[4], J. Allaz[1]

[1]Department of Earth and Planetary Sciences, ETH Zürich, 8092 Zürich, Switzerland, [2]Institute for Integrated Radiation and Nuclear Science, Kyoto University, Kumatori, Osaka 590-0494, Japan, [3]Synchrotron Radiation Research Center, Kansai Institute for Photon Science, National Institutes for Quantum Science and Technology, Sayo, Japan, [4]Department of Environmental Systems Science, ETH Zürich, 8092 Zürich, Switzerland

INTRODUCTION: It is widely accepted most of the terrestrial planets may have experienced one or several phases of magma ocean (MO) stage[1], consequently a portion of silicate melt could still be present in the terrestrial deep mantle as remnants of a primordial MO. For the anomalous velocity structure observed in the ultra-low-velocity-zones[2] atop core-mantle-boundary (CMB) is believed to be due to the presence of such melt. Furthermore, recent seismic evidence indicates the presence of a largely molten silicate layer above the core of Mars[3] indicating that such basal silicate layers may be widespread phenomena among terrestrial planets. Their long-term survival in deep terrestrial planetary interiors is subject to their gravitational stability. However, scarce data on the melt in the relatively low-pressure range force to use silicate glasses as a structural analogue to melt. In this respect we synthesized silicate glasses by laser levitation technique and performed high pressure sound velocity measurements in a diamond anvil cell.

EXPERIMENTS: The starting mixture of the oxides for silicate glass was heated with CO_2 laser on a stage where a gas flow through the nozzle to provide sufficient buoyancy to levitate the molten silicate bead. The sample was melted once at 1900 ± 5 °C to achieve complete fusion. Quenching of the melted silicate leading to the production of a spherical bead. Mössbauer spectra (Fig. 1) were collected on the glass bead at Kyoto University. High pressure sound velocity measurements were carried out at ETH Zurich using Brillouin spectroscopic technique

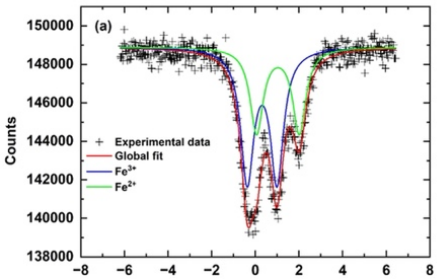

Fig.1: Mössbauer spectrum of the pyrolite-glass with $Fe^{3+}/\sum Fe = 0.61(5)$.

RESULTS: Chemical homogeneity of the glass (pyrolite) was confirmed from the microprobe analysis and Raman spectra. Deconvolution of the room temperature ^{57}Fe Mössbauer spectrum yielded two paramagnetic doublets with respective isomer shift (IS) and quadrupole splitting (QS) of ~1.04(5) and 1.95(5) mm/s attributed to Fe^{2+} and 0.31(5) and 1.36(5) mm/s attributed to Fe^{3+}, consistent with the literature. The area covered by the ferric iron was taken for the calculation of the $Fe^{3+}/\sum Fe$ ratio, which equals to ~0.61(5). The Pressure evolution of the Brillouin spectra is shown in the Fig. 2. A systematic increase in the sound velocity was observed in this study.

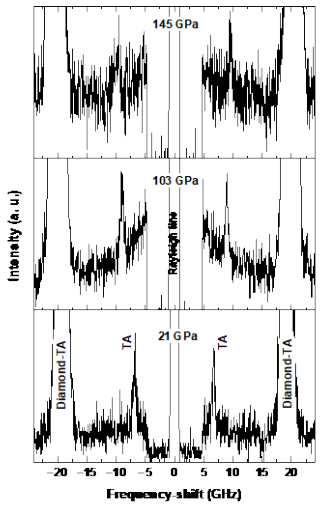

Fig. 2: Representative room temperature Brillouin spectra of pyrolite glass at 21, 103 and 145 GPa. TA represents transverse acoustic mode

REFERENCES:
[1] W. B. Tonks *et al.,* JGR: Planets, **98(E3)**, 5319-5333 (1993).
[2] E. J. Garnero *et al.,* PEPI, **91(1)**, 161-176 (1995).
[3] A Khan *et al.,* Nature, **622(7984)**, 718-723 (2023).